

An Aerostructural Perspective on Winglets

Shahriar Khosravi* and David W. Zingg†

Institute for Aerospace Studies, University of Toronto

4925 Dufferin Street, Toronto, Ontario, M3H 5T6, Canada

This paper presents an aerostructural perspective on the potential benefits of wingletted wings in comparison to planar wings of the same projected span. There is no consensus in the current literature on the efficiency gains possible from winglets. Conclusions made in the past vary significantly depending on the design problem considered and the fidelity of the tools used. The present paper takes a step further towards understanding the tradeoffs in the design of wingletted wings using high-fidelity numerical optimization based on both purely aerodynamic and fully-coupled aerostructural analysis. The high-fidelity analysis in both cases uses the Euler equations to model the flow along with a friction drag estimate based on the wetted surface area. Three configurations are considered: winglet-up, winglet-down, and planar. The results show that winglets oriented downward produce a greater drag reduction than winglets oriented upward for two reasons. First, the winglet-down configuration moves the tip vortex further away from the wing from a purely aerodynamic standpoint. Second, the winglet-down configuration has a higher projected span at the deflected state due to the structural deflections. This indicates that fully-coupled high-fidelity aerostructural optimization is required to quantify the benefits of winglets properly. We present results for two variants of the Boeing 737NG aircraft: B737-600 and B737-900. The winglet-down configuration can reduce the total drag by up to 2% at the same total weight as the optimal planar counterpart. These conclusions are applicable to new wing designs, as opposed to retrofits; the potential efficiency improvements offered by retrofitted winglets may be different.

*Ph.D. Candidate, Corresponding Author, shahriar.khosravi@mail.utoronto.ca

†Professor and Director, J. Armand Bombardier Foundation Chair in Aerospace Flight

Nomenclature

b	Projected wing span	ℓ	Location of wing-winglet junction
b^*	Projected span at the deflected state	M	Freestream Mach number
C_L	Lift coefficient	q_∞	Freestream dynamic pressure
C_p	Pressure coefficient	W	Wing weight
D	Total drag	W_0	Wing weight of the initial design
D_{inviscid}	Inviscid drag	W_{MTO}	Maximum takeoff weight
D_0	Inviscid drag of the initial design	x, y, z	Streamwise, spanwise, and vertical coordinates
e	Span efficiency factor	β	Objective function parameter
g	Gravitational acceleration constant	θ	Winglet cant angle
J	Optimization objective function	ϕ	Dihedral angle
L	Lift		

I. Introduction

The environmental impact of carbon emissions from commercial aviation raises concerns about the future of the airline industry. To sustain the current growth of the industry, commercial airplanes must become highly efficient in terms of fuel consumption. As a result, drag reduction is an important area of research in aviation because aircraft fuel consumption is directly related to drag.

Lift-induced drag (or simply induced drag) is typically 40% of the total drag of a commercial aircraft in cruise [1]. It is therefore worthwhile to explore concepts that reduce the induced drag. This has been the primary motivation for researchers to study nonplanar wings and, in particular, winglets. There have been many studies in the past decades on the possible fuel efficiency improvements provided by winglets. We mention a few important examples in this paper; a more thorough review is provided by Kroo [1].

The term *winglet* was first used by Whitcomb [2] at NASA. He showed that winglets can provide a significant improvement in the lift-to-drag ratio over planar wingtip extensions at the same level of root bending moment. While the winglets and wingtip extensions were designed by a combination of available theory and wind tunnel tests, the wing itself was not redesigned. At the same time, another study done by NASA considered the relative advantages of winglets and wingtip extensions [3]. It concluded that at the same level of root bending moment, winglets provide a greater induced drag reduction than a wingtip extension. Later, another study by Jones and Lasinsky [4] concluded that when optimized wing shapes are considered, similar reductions of induced drag may be achieved either by extending the wingtip or by having a vertical winglet.

Asai [5] studied the relative advantages of planar and nonplanar wings and concluded that the tradeoff between the induced drag and wing root bending moment alone is not enough to determine the effectiveness

of winglets. The effects of the viscous drag penalty incurred by winglets must also be taken into account. He further suggested that if both the root bending moment and viscous drag are kept constant, it is possible to design a planar wing with lower total drag than any nonplanar wing. Van Dam [6] considered planar wings that produce a nonplanar wake at a nonzero angle of attack and suggested that these geometries can provide considerable induced drag reductions. However, much of the improvement was later attributed to numerical integration inaccuracies [7].

More recently, Takenaka and Hatanaka [8] performed a multidisciplinary design exploration for a winglet using high-fidelity computational fluid dynamics (CFD) and computational structural mechanics. They considered a sample of 32 winglets having various root chord lengths, taper ratios, sweep angles, spans, cant angles, and toe angles for multidisciplinary design optimization based on the Kriging model. Their optimized winglet provides a reduction in total drag of approximately 22 drag counts while increasing the wing root bending moment by 5.3%. Furthermore, they demonstrated that a conventional winglet, one that is a vertical extension of the wingtip geometry, can only provide a reduction of 17 drag counts while increasing the root bending moment by 3.5% in comparison to the baseline planar wing. The total drag reductions provided by the wings with winglets were also validated using wind tunnel tests. However, it is important to note that only the winglets were optimized in this study. The shape of the wing was not optimized.

Another notable numerical study, conducted by Verstraeten and Slingerland [9], focused on the drag characteristics of optimally loaded planar wings, wings with winglets, and c-wings using a low-fidelity model of the aerodynamics and weight. They concluded that when a span constraint exists, a wingletted wing with a height-to-span ratio of 28% provides a total drag reduction of 5.4% in comparison to a planar wing at identical wing root bending moments. This study also demonstrated that winglets can be used to provide induced drag reductions when there is a constraint on the aspect ratio of the wing. Ning and Kroo [10] did a similar study, but included the area-dependent weight in their calculations too. They also took into account the effects of a critical structural load factor on the tradeoffs in the design of wings with winglets. Another notable difference in this study was the inclusion of a stall speed constraint. They demonstrated that whether a winglet performs better than a wingtip extension depends on the ratio of the maneuver lift coefficient to the cruise lift coefficient. This is due to the fact that the area dependent weight is a function of the ratio of the maneuver and cruise lift coefficients in the proposed weight model. When this ratio is equal to unity, a wingtip extension is slightly more advantageous while the winglet performs marginally better when this ratio is equal to 2.5. This trend held true for both retrofits and new wing designs. Using a medium-fidelity aerostructural optimization approach, Jansen et al. [11] showed that a wing with a winglet is the globally optimal design when a span constraint exists. Furthermore, when the span is unconstrained, the optimal design is a raked wingtip.

Despite the considerable research effort on this subject, there is still no clear consensus on the ability of nonplanar wingtips to provide significant fuel efficiency improvements, especially for a new wing design, and the conditions under which the potential benefits are seen. Conclusions made in the past vary depending on the specific design problem considered and the level of physical detail that the models used are able to capture. This means that more work needs to be done in order to rigorously quantify the possible efficiency gains from winglets. Furthermore, fully-coupled high-fidelity aerostructural optimization is essential in order to capture the interdisciplinary and nonlinear effects that are important in the study of winglets. The present study contributes to this objective by conducting aerostructural optimization based on the Euler equations with a friction drag estimate based on the wetted surface area during the post-optimality calculations. It is important to note that our goal is not to introduce a new methodology for performing the numerical optimization itself. Instead, we aim to focus on valuable design insights that may not be captured using low- and medium-fidelity optimization tools.

In the study of nonplanar wingtip devices, it is important to make a distinction between retrofitted winglets and new wing designs. A retrofitted winglet is intended as an after-market addition to an existing wing design in an attempt to improve the aerodynamic performance of the wing. There are many examples of retrofitted winglets on today's modern transport aircraft. These include the B737NG, B747-400, B767-400, MD-11, and KC-135. In all of these examples, the addition of a nonplanar wingtip device increases the span of the wing [12]. This is an important consideration when discussing the potential benefits of winglets. It is difficult to rigorously quantify the efficiency improvements of winglets when the projected span of the wing is increased because the induced drag is reduced quadratically with an increase in the span. Therefore, the fact that these retrofitted winglets improve the performance of existing wings may not necessarily mean that new wing designs with winglets will also outperform their planar counterparts of the same projected span. Our present conclusions apply in the context of new wing designs, as opposed to retrofits.

Aerostructural optimization based on the Euler equations is sufficient for studying the main trends involved in the design of wingletted wings. At the end of the optimization, the post-optimality friction drag estimate will ensure that the increase in the wetted surface area as a result of having a winglet is taken into account in calculating the total drag of a wingletted wing. Using this strategy leads to similar trends obtained from high-fidelity aerodynamic shape optimization based on the Reynolds-averaged Navier-Stokes (RANS) equations [13]. Thus, it is not necessary to model the flow based on the RANS equations for the purpose of the current study.

Most of the test cases presented in this paper involve analyzing the lift and drag performance of wings at a single cruise point. As a result, the individual wings obtained from the optimizations will not perform well in other on- and off-design conditions. Conducting multipoint optimization would address this challenge,

but it requires a large amount of computational resources given the high-fidelity nature of the aerostructural analysis. However, a significant amount of insight about the general trends in the relative performance of wingletted and planar wings can still be learned from the present studies.

In the present work, we size the structures based on the von Mises failure criterion at a $2.5g$ load condition. At this stage, we do not consider structural constraints such as buckling and flutter. Although these are important considerations in practical wing design, we believe that neglecting them does not significantly affect our conclusions. Our results could overestimate the benefits of winglets, but are unlikely to underestimate them. Furthermore, we do not consider additional critical structural load conditions in sizing the structures. However, this does not adversely affect our main conclusions because our approach leads to the same structural sizing trends as the ones obtained from studies that include more load conditions [14, 15]. It is important to note that our objective in the present work is to study the main trends, not to perform detailed wing design. The present structural sizing strategy is sufficient for this purpose.

The present study uses a step-by-step approach to studying winglets where purely aerodynamic shape optimization is conducted first before performing fully-coupled aerostructural optimization. This approach is central to understanding the arguments presented in this paper. Therefore, it is worthwhile to provide a brief description of what each individual step is intended to achieve. In Section III.B, we conduct purely aerodynamic shape optimization in order to establish that the numerical tools work as intended and recover the expected trends. Moreover, this section demonstrates that a winglet oriented downward is more effective than a winglet oriented upward, even for purely aerodynamic shape optimization with no deflections. Section III.C presents results from fully-coupled aerostructural optimization for planar and wingletted wings of the same projected span. The main objective is to see what the aerostructural optimizer does given the freedom to choose between a winglet-up and winglet-down configuration starting from an initially planar wing. In Section III.D, we aim to determine what the optimizer chooses to do given the freedom to either keep the wing planar or create a winglet for each configuration. Finally, Section III.E will explore the possibility that a wingletted wing may provide a higher efficiency improvement in high-lift, low-speed conditions where the ratio of the induced to total drag is higher than in cruise. Sections III.B and III.C use the Boeing 737-600 wing as the baseline configuration, and Sections III.D and III.E consider the larger Boeing 737-900 as the baseline design. This will help to gain a better understanding of the sensitivity of the conclusions with respect to different baseline aircraft. The B737-600 and B737-900 aircraft are part of the same family known as the B737NG and have identical planforms. However, they differ in terms of maximum takeoff weight, range, and length of the fuselage. The higher weight of the B737-900 variant leads to a larger induced drag in cruise and may affect the tradeoff between weight and drag.

Our choice of B737NG for the baseline aircraft is justified by the fact that this family represents a signif-

ificant share of today’s commercial flight operations. For instance, data from the United States Department of Transportation shows that the B737NG aircraft alone accounted for 21.1% of the total amount of fuel burned in 2015. In fact, the B737NG aircraft burned more fuel than any other commercial aircraft family in the United States. If we consider the similar Airbus A320 family in addition to the B737NG, the fuel burn percentage rises to 36.5%. This means that any fuel efficiency improvement from winglets for this type of commercial aircraft can make a significant contribution to reducing the environmental footprint of aviation.

II. Methodology

The aerostructural optimization framework used in this work consists of six main components: 1) a multiblock Newton-Krylov-Schur flow solver for the Euler and Reynolds-averaged-Navier-Stokes equations [16, 17], 2) a finite-element structural solver for the analysis and optimization of the structure [18], 3) a mesh movement technique based on the linear elasticity equations for moving the aerodynamic grid during aerostructural analysis and optimization [19], 4) a surface-based free-form deformation (FFD) technique for moving the structures mesh during optimization [20, 21], 5) a B-spline parameterization method for geometry control which is coupled with the linear elasticity mesh movement technique [19], and 6) the gradient-based optimizer SNOPT [22] with gradients calculated using the discrete-adjoint method for the coupled multidisciplinary system. Since the two discipline solvers are written in different programming languages, we use Python to provide an interface for the solvers [23]. Zhang et al. [20, 21] provide a detailed description of the framework in addition to extensive validation and verification studies that establish the validity of the methods used.

The flow solver is based on an efficient parallel multiblock finite-difference methodology that makes use of summation-by-parts operators for the spatial discretization and simultaneous approximation terms for the imposition of boundary and block interface conditions. The solution to the discrete equations at each Newton step is computed using the generalized minimum residual scheme with approximate Schur preconditioning. The one-equation Spalart-Allmaras turbulence model is used to model turbulent flows. All the optimization results presented in this paper are based on the Euler equations. Hicken and Zingg [16] and Osusky and Zingg [17] provide comprehensive details of the flow solver.

The structural analysis is performed by a parallel finite-element code called the Toolkit for the Analysis of Composite Structures (TACS) [18]. It is capable of performing either linear or geometrically nonlinear analysis. However, only linear analysis is considered in this study. TACS is able to handle all of the required design variables for the thickness values of structural components inside the wing box. It is written in C++ and provides a Python interface for straightforward coupling to solvers from other disciplines. Additionally, it has the built-in capability to provide sensitivities with respect to the design variables.

Performing aerostructural analysis and optimization requires transferring the loads and displacements between the aerodynamic and structural solvers. To accomplish this goal, rigid links are constructed between the aerodynamic surface nodes, where the aerodynamic forces are calculated, and the closest points on the structures finite-element mesh [24]. The displacements are then extrapolated from the structures mesh to the aerodynamic surface grid.

The aerodynamic volume grid is parameterized by B-spline tensor volumes. The B-spline control points on the surface of the geometry provide an efficient means for the optimizer to accomplish shape changes during optimization. This geometry parameterization technique is integrated with a linear elasticity mesh movement algorithm [16]. As the B-spline control points that define the surface geometry move, each B-spline tensor volume is treated as a linearly elastic solid, for which a finite-element solution is found to represent its new shape. The updated aerodynamic grid is then recovered from the new B-spline tensor volumes. This integrated geometry parameterization and mesh movement technique parameterizes both the undeflected aerodynamic geometry and the deflected flying shape.

When the optimizer changes the aerodynamic geometry, the internal structure of the wing must also move in order to reflect the new shape. This framework uses a surface-based FFD method that parameterizes the space enclosed between the B-spline surfaces [20, 21]. The internal structures of the wing are then embedded inside this space between the upper and lower surfaces of the aerodynamic geometry. Thus, as the aerodynamic geometry is changed by the optimizer, the internal structures move with it in a consistent manner.

A gradient-based optimizer is used for optimization because gradient-based optimizers typically require fewer function evaluations than genetic algorithms [25]. Consequently, all optimized geometries presented represent local minima which may not be the global minimum [26]. Although we have not conducted a formal investigation on the degree of multimodality in fully-coupled high-fidelity aerostructural optimization problems, we have tried a few cases using multiple initial geometries. These cases suggest that the design spaces are unimodal. The gradients of the objective and constraints are computed using the coupled adjoint method outlined by Martins et al. [27]. The adjoint method is efficient for problems with many more design variables than constraints because the cost of computing the gradient is nearly independent of the number of design variables. We use the gradient-based sequential quadratic programming optimization algorithm SNOPT, which allows for the solution of large-scale constrained problems [22]. PyOpt [23] is used to provide a Python interface for SNOPT.

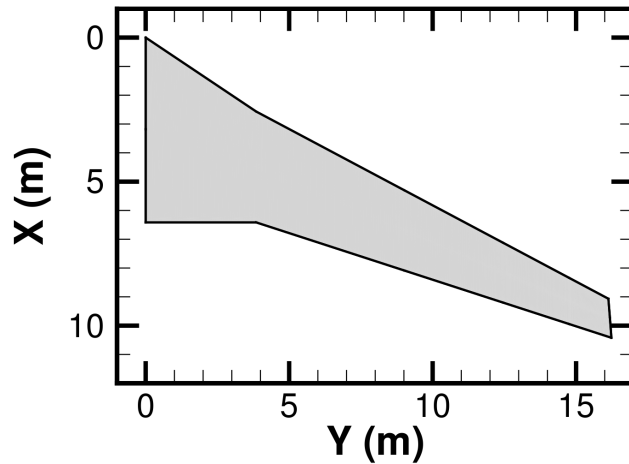


Figure 1: The planform of the baseline planar configuration is based on the Boeing 737NG. Only the wing is considered for shape optimization.

III. Results and Discussion

III.A. Baseline Geometry

The baseline wing geometry for this study is loosely based on the planform of the Boeing 737NG wing shown in Figure 1 with the RAE 2822 supercritical airfoil. All of the wingletted and planar configurations have the same projected span. There are two main reasons for constraining the projected span. First, we are assuming that there is an airport gate constraint that prohibits any increase in the span relative to the baseline wing. Second, if the wingletted wings grow in span, then it will not be clear whether any aerodynamic benefit is due to the increased span or the nonplanar feature. This is due to the fact that, based on linear aerodynamic theory, the induced drag is reduced in a quadratic fashion with any increase in wing span [28].

The Boeing 737NG aircraft with winglets have a span that is 4.5% larger than the span of the Boeing 737NG without winglets [29]. According to linear aerodynamic theory, the total drag reduction in cruise as a result of the same span increase is approximately 4%. The Boeing Commercial Airplanes company claims a 3% to 4% total cruise drag reduction for the wingletted wings in comparison to the baseline planar wing [12]. As a result, it is not clear how much of this improvement is due to the winglet alone. This is one of the main reasons that we do not allow our wingletted wings to grow in span relative to the planar configuration. We constrain the undeflected projected wing span in all cases to a value of 106 ft. Thus, we should be cautious in comparing the potential aerodynamic performance improvement from this investigation with the values published for the Boeing 737NG blended winglets since the latter involve an increase in span.

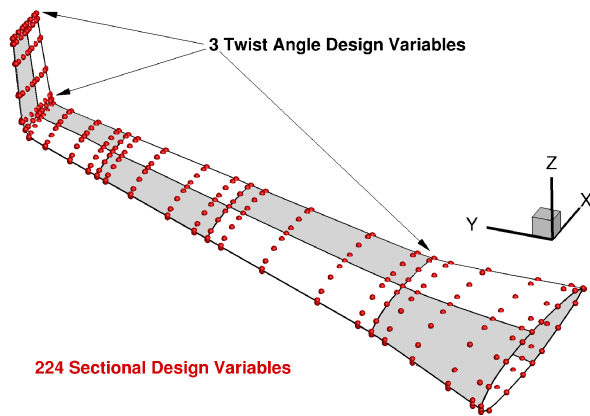


Figure 2: The geometric parameterization and design variables for the winglet-up configuration.

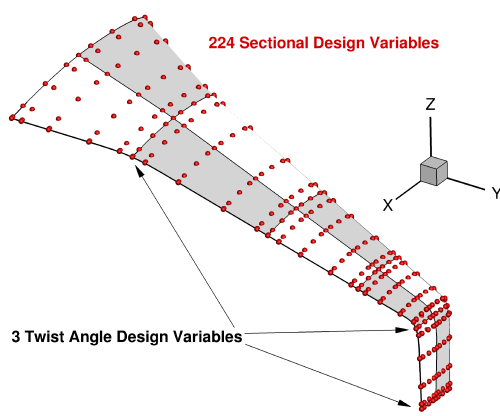


Figure 3: The geometric parameterization and design variables for the winglet-down configuration.

III.B. Aerodynamic Shape Optimization

Although the primary focus of the present paper is on using high-fidelity aerostructural analysis and optimization, it is insightful to begin this investigation on winglets by conducting purely aerodynamic shape optimization. This step-by-step approach, where the optimization studies are first performed using high-fidelity aerodynamic analysis based on the Euler equations, will lead to a solid understanding of the best-case scenario for wingletted wings. It also helps to establish the methodology used by reproducing similar trends observed in previous studies [13, 30, 31]. In this section, we will show that the benefits of winglets are smaller for transonic wings of fixed span than might appear from studies of wings at lower speeds. Furthermore, we will provide evidence that the winglet-down configuration offers a larger drag reduction than the winglet-up design in the context of purely aerodynamic shape optimization.

There are three configurations considered in this study: winglet-up, winglet-down, and planar. All three configurations have identical projected spans. Figures 2 and 3 show the geometric parameterization and design variables for the winglet-up and winglet-down cases, respectively. Each surface patch on the geometry is parameterized by 6×6 B-spline control points. There are a total of 252 section control points of which 224 are design variables. The coordinates of the remaining control points are a function of the neighboring design variables such that slope continuity is maintained over the entire surface of the wing. The optimizer has the freedom to change the sectional shape of the wing by manipulating the z -coordinates of the control points at all spanwise stations across the wing and winglet. The winglet cant angle is constrained to $+71^\circ$ for the winglet-up, and -71° for the winglet-down configuration. (The cant angle of the Boeing 737NG blended winglets is equal to $+71^\circ$.) The planar configuration has a cant angle of zero. In each case, the wing sweep and winglet cant angles are fixed. As a result, only the sectional shape and twist distribution of the wings and winglets are free to vary over the course of the optimization. The thickness-to-chord ratio of the wing and winglet cannot reduce by more than 30%. However, the volume of the wing is constrained to the initial

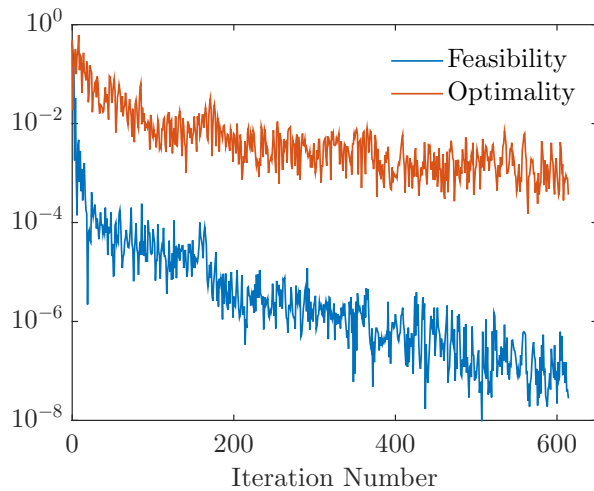


Figure 4: The convergence of optimality and feasibility measures for the winglet-up aerodynamic optimization case.

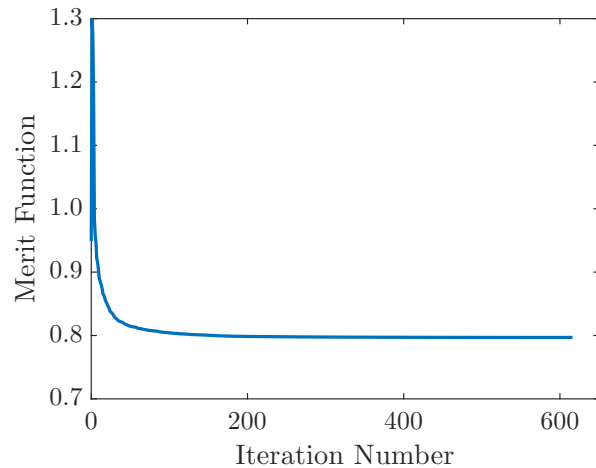


Figure 5: The convergence of the Lagrangian merit function for the winglet-up aerodynamic optimization case.

value to avoid unrealistic designs.

The objective function is the inviscid drag of the wing in cruise. The cruise Mach number is $M = 0.785$ at an altitude of 35,000 ft. In all three cases, the lift constraint is set to $C_L = 0.486$. This lift constraint is based on performing a fully-coupled aerostructural optimization for a planar wing. The aerodynamic optimizations are performed on a grid with 653,184 nodes. This grid does not have sufficiently fine grid spacings for accurate prediction of drag, but is able to capture the dependence of drag on the geometry. The final optimal geometry is analyzed using a grid with 36,793,008 nodes to provide a more accurate estimate of the final objective function values during the post-optimality analysis. Figures 4 and 5 show the optimization convergence for the winglet-up case. Feasibility is a measure of the largest nonlinear constraint violation, and optimality is a measure of the gradient. The merit function is equal to the objective function when all nonlinear constraints are satisfied to machine precision. For a well-converged optimum, both measures must be as low as possible. It is clear from Figures 4 and 5 that the optimization problem has converged to an optimal design. An important secondary conclusion is that the optimizer achieved the majority of the reduction in the merit function over the first 200 iterations. This provides some practical justification for ending the optimization once the majority of the merit function reduction is achieved, especially in high-fidelity optimization where the cost of a function evaluation and the corresponding gradient calculation is high.

Figures 6, 7, and 8 show the optimal lift distributions obtained for the planar, winglet-up, and winglet-down configurations, respectively. The lift distribution for the planar wing closely follows the elliptical load suggesting that the optimizer has minimized the induced drag. The optimal spanwise lift distributions for the winglet-up and winglet-down configurations have a higher tip loading in comparison to the planar case.

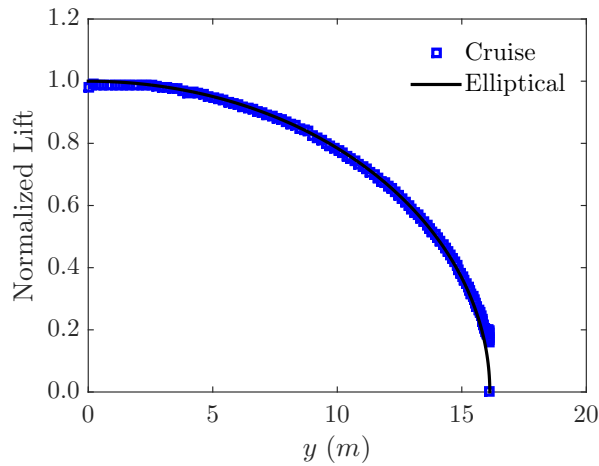


Figure 6: The aerodynamically optimal lift distribution for the planar configuration.

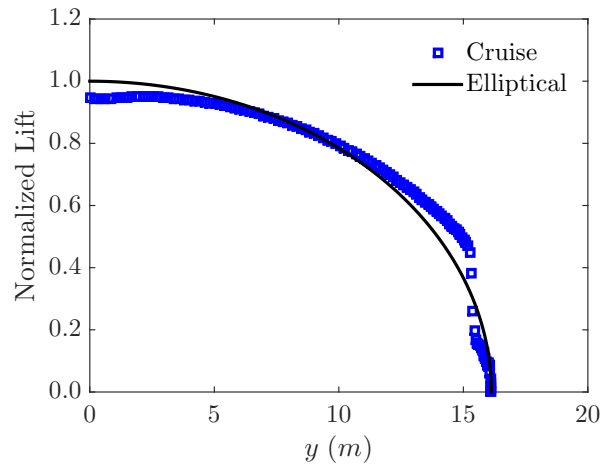


Figure 7: The aerodynamically optimal lift distribution for the winglet-up configuration.

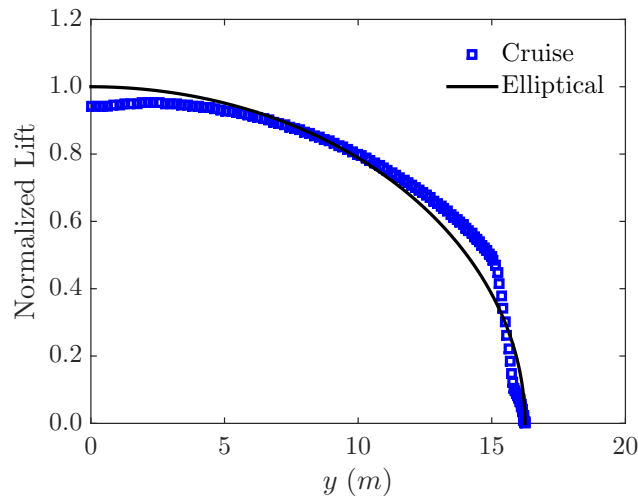


Figure 8: The aerodynamically optimal lift distribution for the winglet-down configuration.

This is consistent with previous studies that show aerodynamically optimal wingtip devices tend to increase the tip loading [12, 30, 31]. This increase in tip loading has important implications in terms of wing weight that are ignored by the aerodynamic shape optimizer. A higher tip loading tends to increase the weight of the wing by requiring a heavier root structure to support the greater moment. Figure 9 shows plots of pressure coefficient along the span for the optimized winglet-up and winglet-down configurations.

Figure 10 provides a comparison of the total drag in cruise between the wingletted and planar wings. A post-optimality friction drag estimate of the entire aircraft is included in each case based on the wetted surface area in order to account for the increased friction drag of the wingletted configurations as a result of the larger surface area in comparison to the planar wing. For the baseline aircraft, we use the Vehicle Sketch Pad modeling tool developed at NASA Langley Research Center [32] to estimate that the friction drag at cruise is equal to 192 drag counts. The larger friction drag for the wingletted wings is taken into account

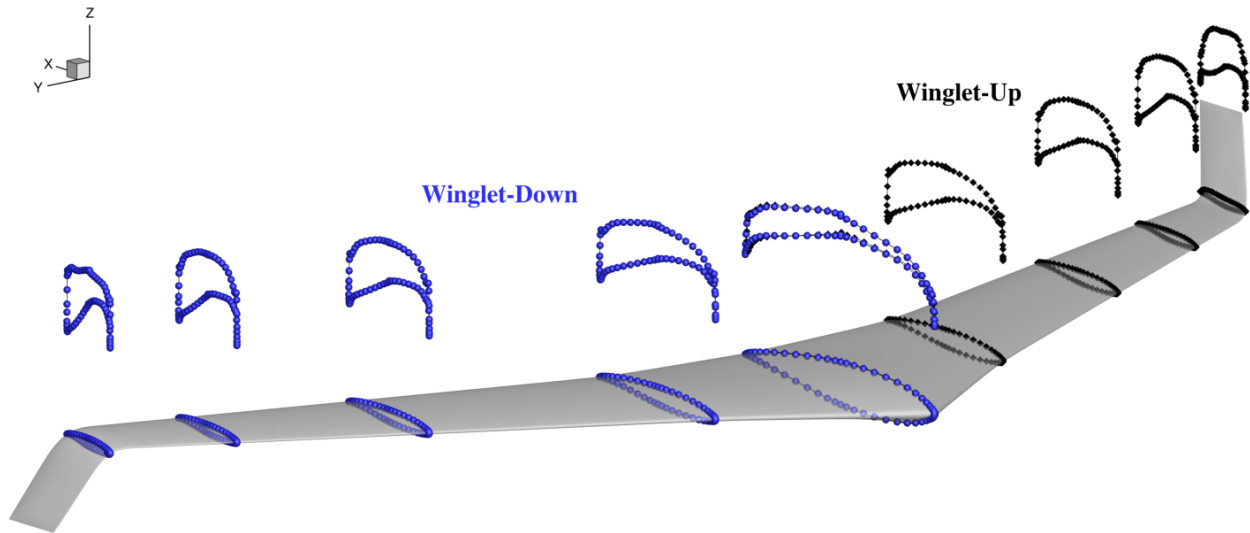


Figure 9: Plots of pressure coefficient in cruise condition for the optimized winglet-up and winglet-down configurations.

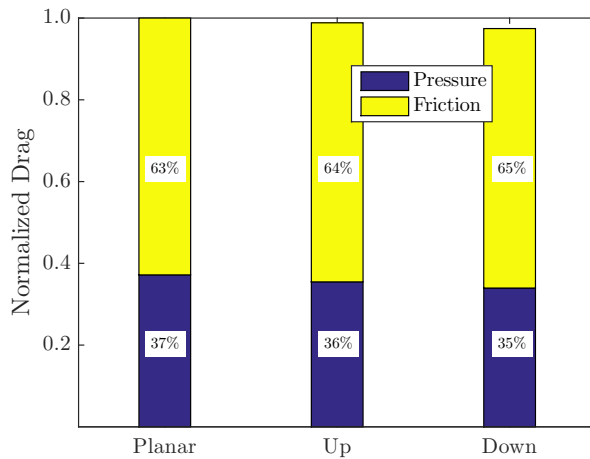


Figure 10: Comparison of total drag in cruise for the planar and wingletted wings, including the proportions of pressure and friction drag.

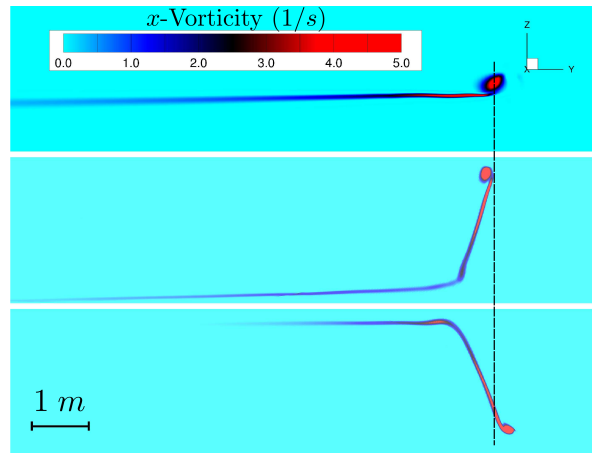


Figure 11: Contours of x -vorticity behind the trailing edge of the wing for all three cases.

based on the increase in the wetted surface area relative to the baseline case [33]. Figure 10 indicates that the winglet-up configuration provides a 1.1% total drag reduction in comparison to the planar wing of the same projected span. The reader is reminded that, unlike the B737NG wings with blended winglets, these wingletted wings have the same projected span as the planar wing. Hence the benefit of the winglet is smaller than that achieved when the winglet leads to a span increase. It is also noteworthy that the optimal winglet oriented downward produces a drag reduction of 2.6% relative to the planar wing, more than twice that of the optimal winglet oriented upward. In order to examine why the winglet-down configuration produces a larger benefit, it is insightful to plot contours of x -vorticity behind the trailing edge of the wing in each case. As shown in Figure 11, these provide some insight into the physical mechanism by which induced drag is generated. Figure 11 shows that the winglet-down configuration is able to push the tip vortex further away

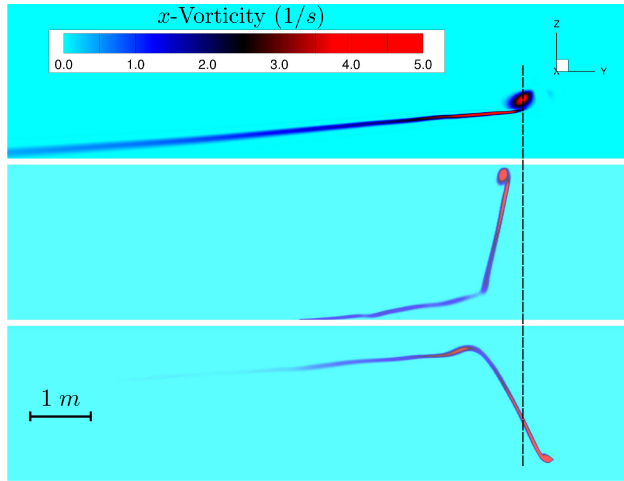


Figure 12: Contours of x -vorticity at the deflected state for all three cases.

from the wake of the wing in the positive y -direction, as indicated by the dashed line. This means that the induced velocity (downwash) on the wing is minimized because it has an inverse relation with the distance from the center of the vortex core [28]. This phenomenon has also been observed in other optimization studies using the Euler [34] and Reynolds-averaged Navier-Stokes equations [13], where the winglet-down configuration is shown to provide a larger drag reduction in comparison to an optimal winglet-up design.

The results shown in Figure 11 are obtained from purely aerodynamic shape optimization, ignoring the effects of structural deflections. Before we turn to fully-coupled aerostructural optimization, it is insightful to examine how the x -vorticity distribution changes in each case when the structural deflections are taken into account. This is shown in Figure 12. In the case of the winglet-up configuration, the inboard deflection of the winglet feature brings the tip vortex closer to the wing relative to the purely aerodynamic case. This can reduce the effectiveness of this configuration from an aerostructural standpoint. On the other hand, the winglet-down configuration has an outboard deflection and pushes the tip vortex even further away from the wing relative to the purely aerodynamic case. Therefore, capturing the structural deflections is essential as it may have a significant effect on our conclusions on the possible efficiency gains from winglets.

III.C. Aerostructural Optimization with Variable Winglet Cant Angle

This section presents results obtained from fully-coupled high-fidelity aerostructural optimization, where the effects of weight and structural deflections are taken into account in addition to drag. The baseline geometry is still based on the Boeing 737NG planform shown in Figure 1 with the RAE 2822 airfoil section. We consider the same three configurations as before: winglet-up, winglet-down, and planar. The projected span is constrained in all cases. The optimizer is free to vary the wing sweep and winglet cant angles in addition to the section shape and twist distribution of the wing along the span, as shown in Figure 13. Note that in

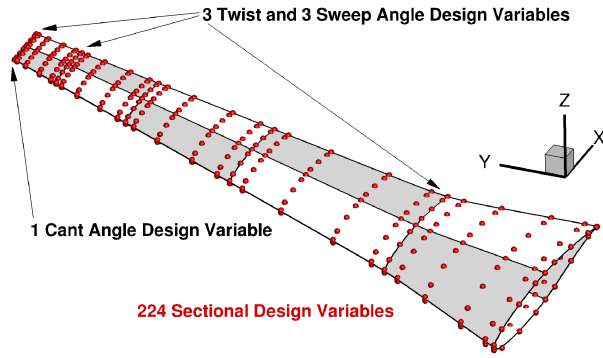


Figure 13: The geometric parameterization and design variables for the exploratory winglet optimization case.

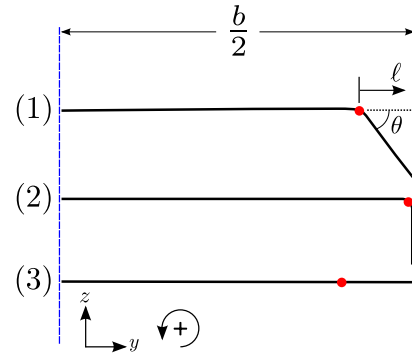


Figure 14: Three possible wing shapes permitted by the parameterization. (1) and (2) are winglet-down, and (3) is planar.

this case, the optimizer is free to choose the optimal wingtip configuration by varying the cant angle design variable. For a winglet configuration to form from the initially planar wing, the cant angle is allowed to vary between -90° and $+90^\circ$. The structure moves consistently with the changes in the winglet cant angle by the means of the surface-based FFD technique for structural mesh movement [20, 21]. A positive cant angle corresponds to a winglet-up and a negative cant angle to a winglet-down configuration. The optimizer is also free to keep the wing planar by forcing the cant angle to be equal to zero. The vertical height of the wingletted feature can increase by up to 6% of the wing span. To further clarify this, Figure 14 shows a simplified front view of three possible wing shapes permitted by this particular parameterization. The parameter θ represents the cant angle. In all cases, the projected span of the wing at the undeflected state remains constant even though the optimizer is free to move the location of wing-winglet junction along the span. In Figure 14, the wing-winglet junction is depicted by a red circle, and its physical location along the span is measured by the parameter ℓ .

The choice of the objective function significantly influences the final optimized design. For practical design of wings, the objective is carefully chosen based on the operating requirements for a particular aircraft. However, our main goal in this study is not to discover the best wing for a particular commercial airplane. Instead, we are interested in the fundamental tradeoffs between drag and weight that are involved in the design of wings with winglets. For this reason, we choose an objective function of the form

$$J = \beta \frac{D_{\text{inviscid}}}{D_0} + (1 - \beta) \frac{W}{W_0} \quad (1)$$

where β is a parameter between zero and unity, D_{inviscid} is the inviscid drag of the wing in cruise, W is the calculated weight of the wing satisfying the structural failure constraints at the $2.5g$ load condition, and D_0 and W_0 are the respective initial values. As we vary β from zero to unity, we place more emphasis on drag and less on weight. This allows us to focus on the most relevant aspects of aerostructural design for various

geometries and gain insight into the fundamental tradeoff between weight and drag. Two values for β have been chosen: 0.5 and 1.0. The same friction drag estimate as the one used in Section III.B is included in the post-optimality calculations [32, 33].

Table 1 lists the constraints for each optimization test case considered in this study. There are two lift constraints; one corresponds to the cruise load condition, the other to a 2.5g load condition. The cruise condition is $M = 0.785$ at an altitude of 35,000 ft, while the 2.5g load condition is $M = 0.798$ at an altitude of 12,000 ft. Since the weight of the wing is a function of the structural thickness values, it changes over the course of the optimization. The total weight of the aircraft is assumed to be equal to the computed weight of the wing plus a fixed weight of approximately 650,000 N. This fixed weight is estimated based on the maximum takeoff weight of a Boeing 737-600 discounted by the approximate wing weight. The wing weight is approximately equal to 8.5% of the maximum takeoff weight.

In practical wing design, the structures are sized based on many critical structural load conditions in order to ensure the structural integrity of the wing. The structural sizing has a profound effect on the aerodynamic performance of the wing. By considering a single 2.5g load condition, we aim to capture some of the effects of structural sizing on the tradeoff between drag and weight [11, 24, 35]. This means that we must constrain the calculated stresses on the structures at the 2.5g load condition to prevent structural failure. The finite-element model of the primary wing structures used for these optimization test cases has 30,473 elements. We do not constrain each individual element's stress value because this would require the solution of the corresponding number of coupled adjoint systems. Thus, the stresses are aggregated using the Kreisselmeier-Steinhauser (KS) technique [36, 37, 38]. This stress aggregation approach leads to a conservative structural design. Three KS constraints with a weighting parameter of 30 are used at the maneuver condition: one for the ribs and spars, one for the top skin, and one for the bottom skin. We use a material based on 7075 Aluminum with a Poisson's ratio $\nu = 0.33$ and Young's modulus $E = 70$ GPa. The yield stress is $\sigma_{YS} = 434$ MPa, and a safety factor of 2.0 is applied. In practical design of aircraft, a safety factor of 1.5 is often applied to this specific load condition. However, since we are only considering a single structural load case, it is appropriate to apply a higher safety factor in order to better capture the correct trends in structural sizing of the wing.

Table 2 provides a list of the design variables used in each case. These cases have a total of 389 design variables that control the angle of attack, geometric shape, and structural thickness distribution of the wing. There are two angle of attack design variables: one for cruise, the other for the 2.5g load condition.

Figure 15 shows the layout of the primary structural components in relation to the outer mold line of the wing. Skin elements are not shown for clarity. The root section is at the intersection with the fuselage. The structural layout does not include the leading and trailing edges because the current model cannot accurately

Table 1: Nonlinear constraints used for optimization in all cases

Constraint	Description
Cruise	$L - W_{\text{MTO}} = 0.0$
Maneuver	$L - 2.5W_{\text{MTO}} = 0.0$
Top Skin	$KS \leq 1.0$
Bottom Skin	$KS \leq 1.0$
Rib/Spar	$KS \leq 1.0$
Wing Span	$b = 106 \text{ ft}$
Total	6

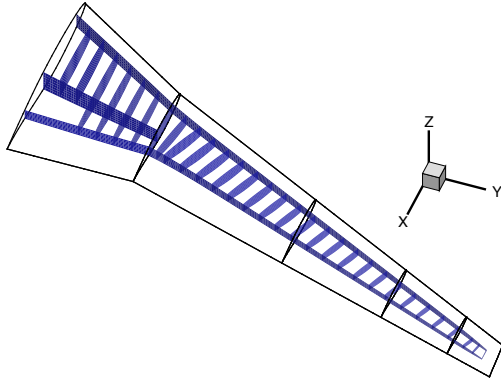


Figure 15: Primary structural layout of the wing in relation to the outer mold line. The wingbox ends at approximately 98% span.

Table 2: Optimization design variables for all cases

Design Variable	Quantity
Twist Angle	3
Sweep Angle	3
Cant Angle	1
Section Shape	224
Angle of Attack	2
Skin Thickness	60
Spar Thickness	66
Rib Thickness	30
Total	389

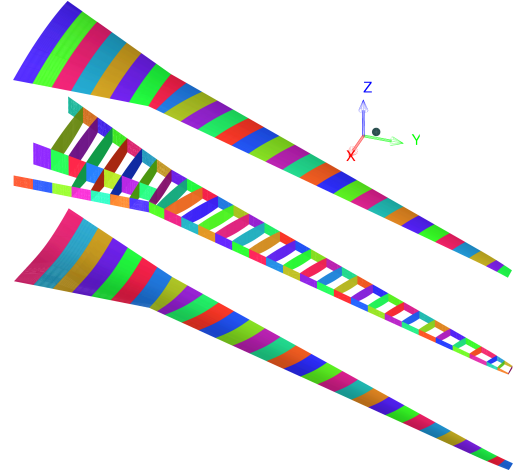


Figure 16: Each colored surface represents a structural component, the thickness of which is a design variable.

represent them. This does not adversely affect our conclusions because these secondary wing structures do not carry a significant amount of load in comparison to the primary structural components. Furthermore, their weight is mostly dependent on the wing projected area [10], which remains constant in our study. The primary components consist of 30 ribs, 3 spars, and 60 skin patches. The structural design variables are the thickness values of these components. Figure 16 shows every component for which there is a thickness design variable. The thickness of each component can vary between 5 mm and 50 mm. The displacements and rotations of the structural model at the root section are fixed, as shown in Figure 17.

These large aerostructural optimization cases are challenging to converge due to the presence of hundreds of design variables and many nonlinear constraints [39]. In order to reduce the difficulties associated with convergence, we first perform the optimizations on a coarse computational fluid dynamics (CFD) mesh with 193,536 nodes. After 240 optimization iterations on the coarse grid, the merit function plateaus and the optimization is continued on a finer mesh with 653,184 nodes in 112 blocks. This aerodynamic grid

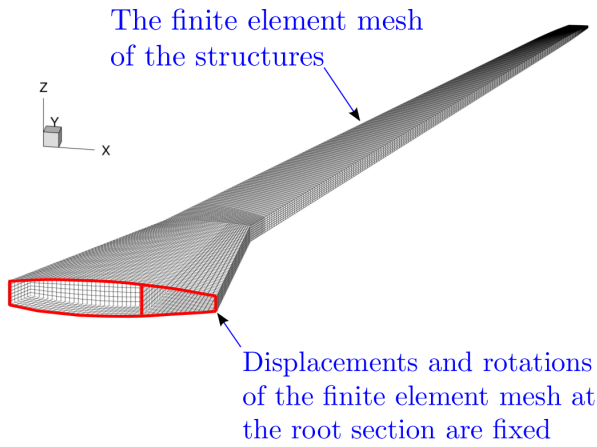


Figure 17: Displacement and rotation boundary conditions for the structures finite element mesh.

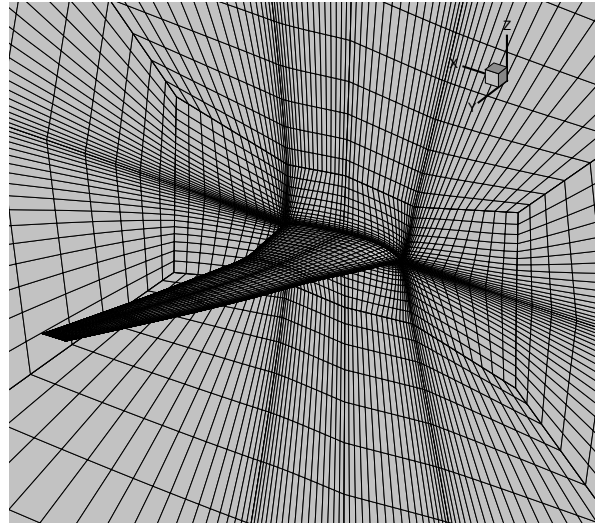


Figure 18: Grid resolution of the surface and symmetry plane for the fine optimization mesh.

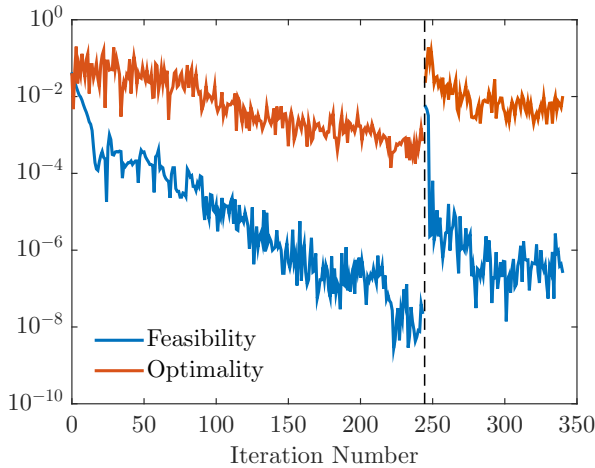


Figure 19: Convergence of optimality and feasibility measures for the winglet-down aerostructural optimization case.

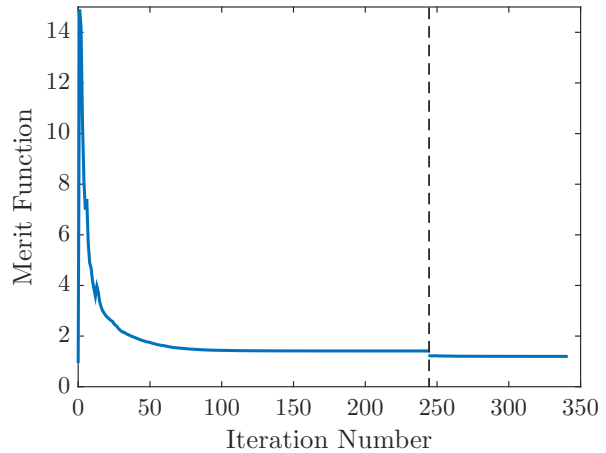


Figure 20: Convergence of the Lagrangian merit function for the winglet-down aerostructural optimization case.

does not have sufficiently fine spacings for very accurate estimations of drag. Thus, we analyze each final optimized design using a more refined CFD mesh with 37 million nodes in order to obtain more accurate drag estimations for the tradeoff curves. It is important to evaluate the final optimized designs on a fine CFD mesh because we would like to ensure that any relative performance benefit obtained on the optimization grid translates in the same way to the fine mesh. Performing the optimizations using this aerodynamic grid is appropriate because, although the grid is too coarse to predict drag accurately, we have verified that the dependence of the drag on the geometry is accurately captured [30]. Figure 18 shows shows the grid resolution of the surface and symmetry plane for the fine optimization mesh with 653,184 nodes.

Figures 19 and 20 show the aerostructural optimization convergence trends for the winglet-down config-

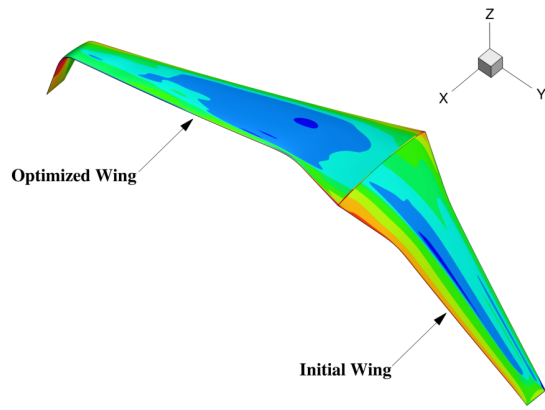


Figure 21: The initial and optimized wing shapes for the $\beta = 0.5$ case.

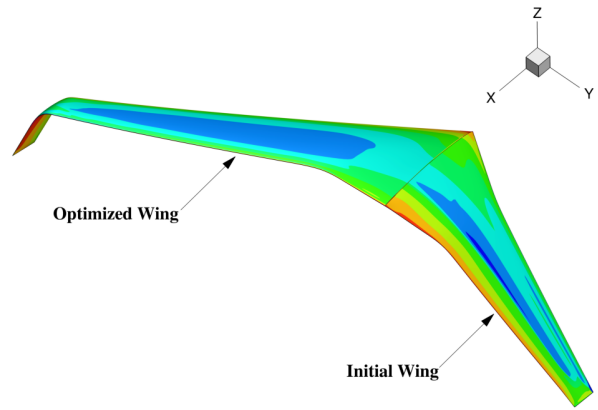


Figure 22: The initial and optimized wing shapes for the $\beta = 1.0$ case.

uration with $\beta = 1.0$ using the coarse and fine optimization grids. The dashed line marks the beginning of the optimization using the fine grid. At the end of the optimization using the coarse grid, the optimized geometry is used as the initial design for the subsequent fine optimization. On the finer aerodynamic grid, the optimizer achieves a further merit function reduction of around 2.2% in 103 function evaluations and satisfies the nonlinear constraints to a tolerance of 10^{-6} . The reduction in optimality on the fine grid is around an order of magnitude, but the fact that the merit function has plateaued means that the majority of the reduction in the merit function is already achieved. These trends hold true for the rest of the cases as well.

Figures 21 and 22 show the optimal winglet configurations for the $\beta = 0.5$ and $\beta = 1.0$ cases, respectively. In both cases, the optimization leads to a winglet-down configuration. It is important to note that the optimizer does have the freedom to vary the cant angle and choose between a winglet-up, winglet-down, or planar configuration. Thus, the winglet-down configuration has better performance in comparison with planar and winglet-up configurations of the same projected span regardless of the value of β . The cant angle of the optimized winglet is equal to -90° in both cases. As an example, Figure 23 shows the contours of the von Mises failure criterion along the span for the winglet-down configuration with $\beta = 0.5$ at the $2.5g$ load condition.

Figure 24 shows plots of the pressure coefficient along the span for the initial and optimized wings on the fine optimization grid. The initial geometry is not shock-free as indicated by the rapid pressure drop at half-chord over a large region of the upper surface of the wing. The initial pressure distribution is produced by the starting geometry at an angle of attack of 2° . Note that the initial design simply serves as a starting point for the optimization and is not meant to yield good lift and drag performance. The optimizer has

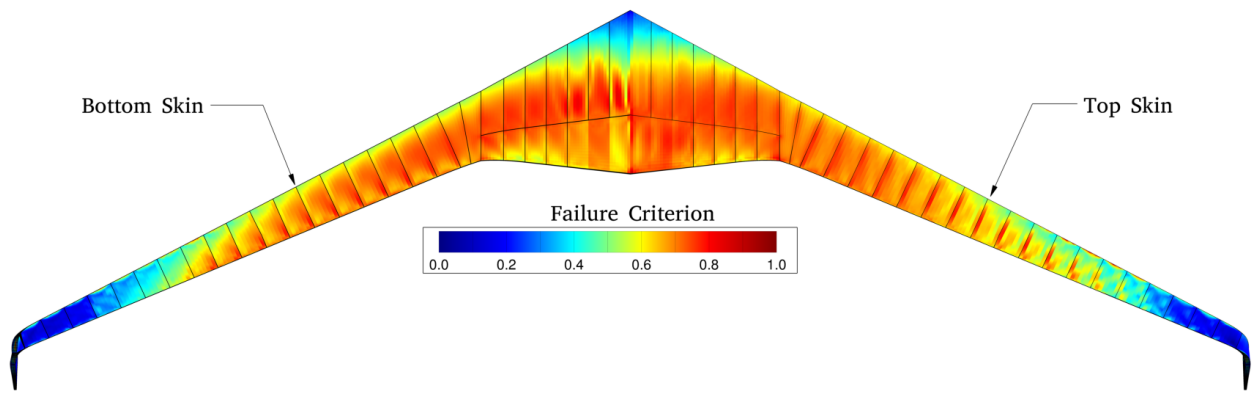


Figure 23: Contours of the von Mises stress criterion at the 2.5g load condition for the optimized winglet-down configuration with $\beta = 0.5$.

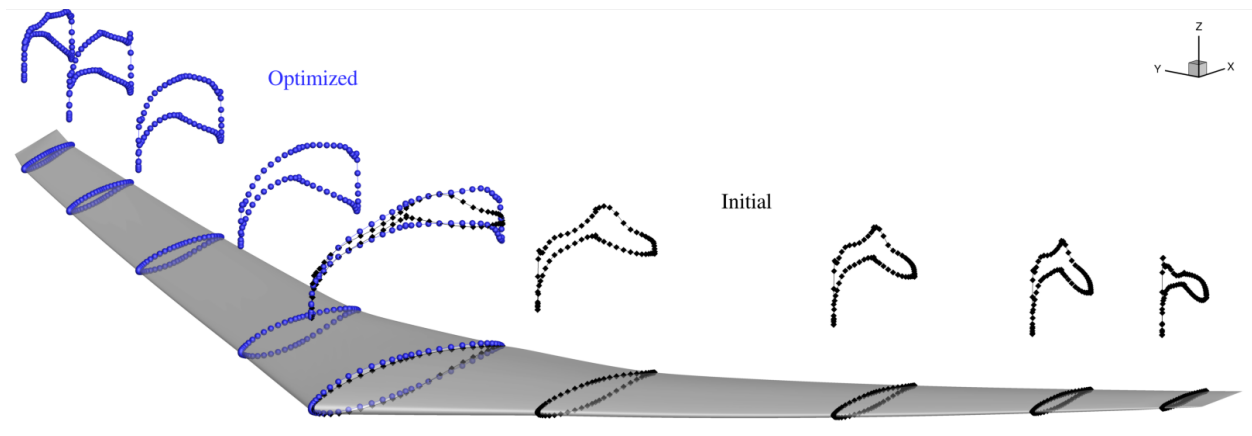


Figure 24: Plots of the pressure coefficient in cruise condition for the optimal planar wing with $\beta = 1.0$.

eliminated the associated wave drag by eliminating the shocks. The rapid pressure recovery near the trailing edge is typical for inviscid optimizations that ignore separation [40]. Ignoring viscous effects does not affect our main conclusions because if wingletted wings do not provide significant drag reductions in inviscid flow, then it is unlikely that their potential improvements will increase in the presence of viscous effects.

Figures 25 and 26 show the optimal lift distributions for the winglet-down configuration for both values of β . With $\beta = 0.5$, i.e. when there is equal emphasis on both weight and drag of the wing in the objective function, the optimal cruise lift distribution is more triangular than the elliptical load. At the 2.5g load condition, the spanwise lift distribution is much more triangular with a significant amount of tip load relief. In fact, the tip loading at the maneuver condition is lower than at cruise. When the objective function is equal to the inviscid drag, i.e. $\beta = 1.0$, the optimal cruise lift distribution more closely follows the elliptical load than the $\beta = 0.5$ case, which is consistent with the expected trend. The optimizer still reduces the tip loading at the 2.5g load condition down to the cruise level by introducing washout near the tip at the deflected state. These plots indicate that the optimizer is actively taking advantage of aeroelastic tailoring. Furthermore, it establishes the fact that the methodology used is able to capture the expected trends.

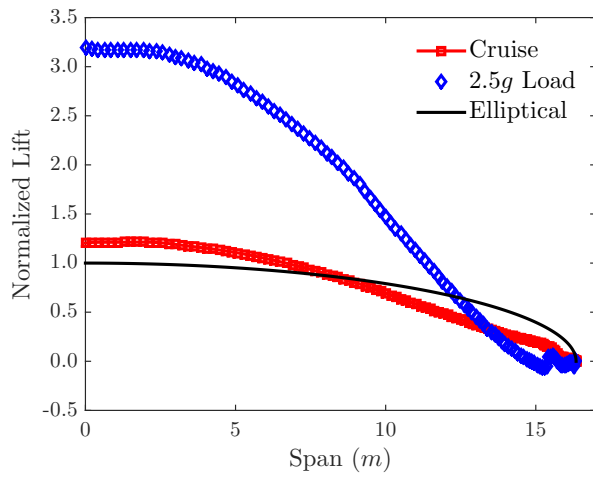


Figure 25: Lift distributions for the optimized winglet-down configuration with $\beta = 0.5$.

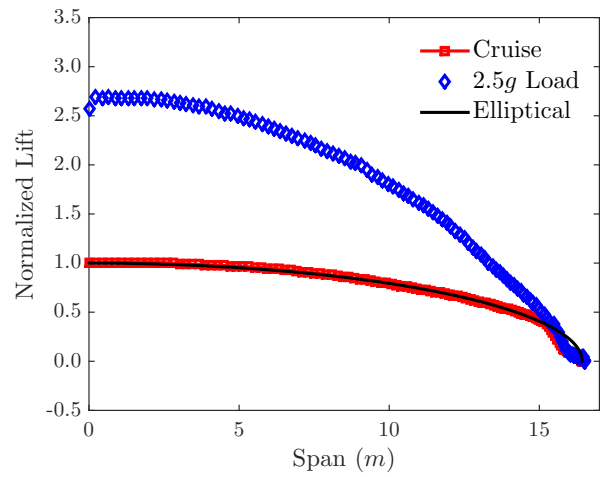


Figure 26: Lift distributions for the optimized winglet-down configuration with $\beta = 1.0$.

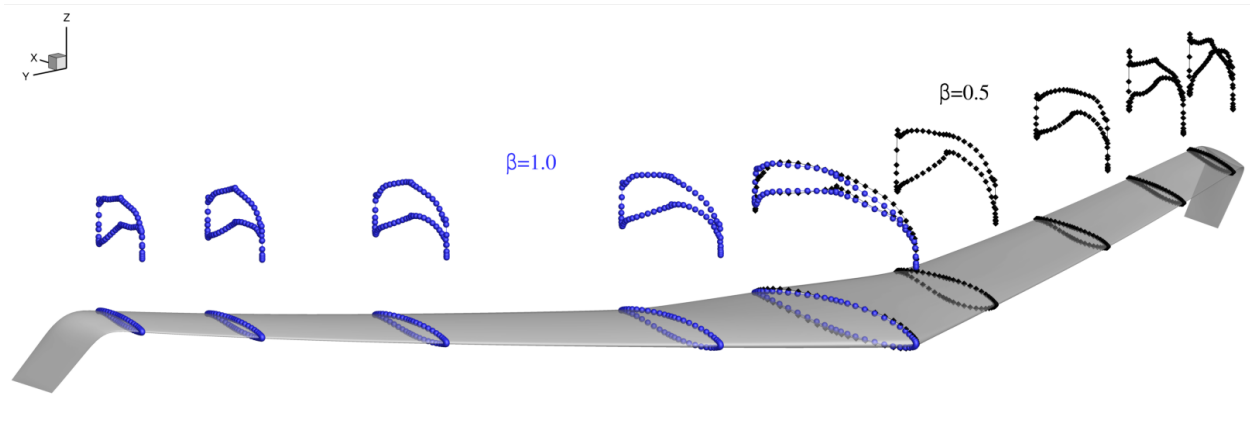


Figure 27: Plots of the pressure coefficient in cruise condition for the optimal winglet-down configurations.

It is insightful to see how the optimizer achieves differences in optimal span loading through aeroelastic tailoring for different values of β . Figure 27 shows plots of the pressure coefficient along the span for both cases. With $\beta = 0.5$, the pressure coefficient curves for the upper and lower surfaces near the wing-winglet junction cross over. This indicates that the force near the leading edge is downward, but it switches direction after the cross-over point. This results in more washout near the wingtip than the $\beta = 1.0$ case. We can see evidence of the differences in the corresponding twist distributions along the span as shown in Figure 28. It is clear that the optimizer is introducing greater washout towards the tip for the $\beta = 0.5$ case. This is consistent with our expectation because with $\beta = 0.5$, there is equal emphasis in the objective function on weight and drag. As a result, the optimizer should reduce the tip loading and shift the load inboard in order to maintain a lighter structure than the $\beta = 1.0$ case. Note that the twist angle at the tip of the winglet in Figure 28 is equivalent to the toe angle and partly controls the loading on the winglet, which in turn determines the structural deflection (bending) of the winglet. We will later on demonstrate that the

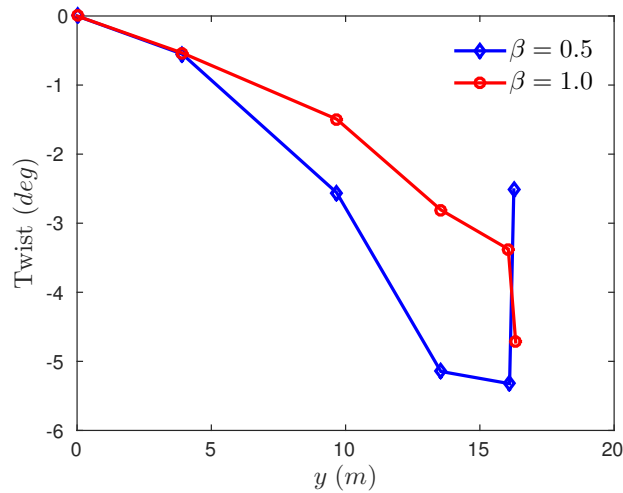


Figure 28: The wing twist distributions in cruise condition for the optimal winglet-down configurations.

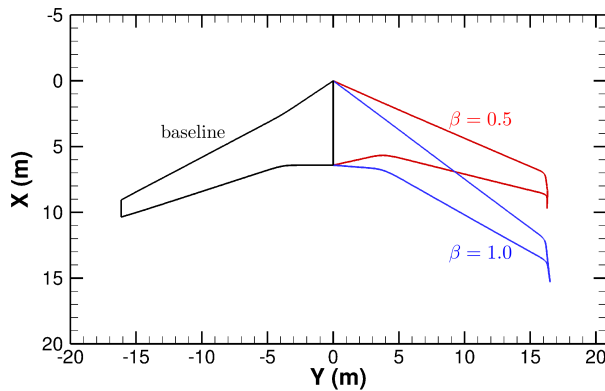


Figure 29: The initial and optimized planform shapes for the aerostructural optimization cases with $\beta = 0.5$ and $\beta = 1.0$.

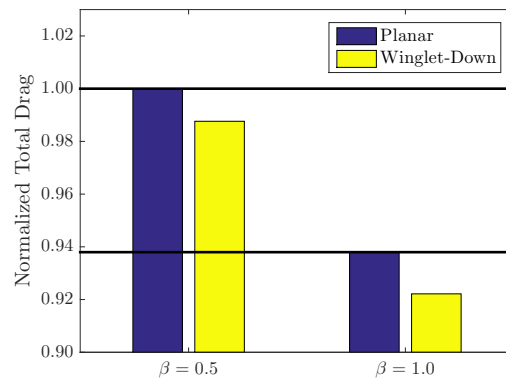


Figure 30: Comparison of total drag between the optimized planar and the optimized winglet-down configuration.

deflection of the winglet is important to consider for induced drag comparisons because it influences the tip vortex location.

It is clear from Figure 29 that the optimizer takes advantage of the geometric freedom in terms of planform in both cases. With $\beta = 0.5$, the overall sweep angle is lower than the case with $\beta = 1.0$. As the emphasis on drag in the objective function is increased, the optimizer increases the sweep angle in order to remove the shocks that are present in the $\beta = 0.5$ case. This is consistent with the expected trend because with increasing β , the weight growth as a result of the larger sweep angle has a smaller influence on the objective function.

Figure 30 provides a comparison of drag between optimized planar wings with a fixed cant angle of zero and the optimized winglet-down configurations with a variable winglet cant angle for both values of β . The drag improvement relative to the planar wing is up to 1.7%. It is clear that in both cases, the winglet-down configuration has lower drag than the optimized planar counterparts. Table 3 provides a summary of the

Table 3: Summary of the cruise point performance of the planar and wingletted wings from aerostructural optimization evaluated on the fine grid

<i>Parameter</i>	Planar		Winglet-Down	
	$\beta = 0.5$	$\beta = 1.0$	$\beta = 0.5$	$\beta = 1.0$
C_L	0.472	0.478	0.473	0.488
Total drag (counts)	321	301	317	296
ΔD	0.0%	0.0%	-1.3%	-1.7%
L/D	14.7	15.9	14.9	16.5
Δb^*	0.0%	0.0%	1.2%	1.8%
$W (\times 10^5 \text{ N})$	2.49	3.96	2.61	5.07
e	0.814	0.984	0.881	1.138

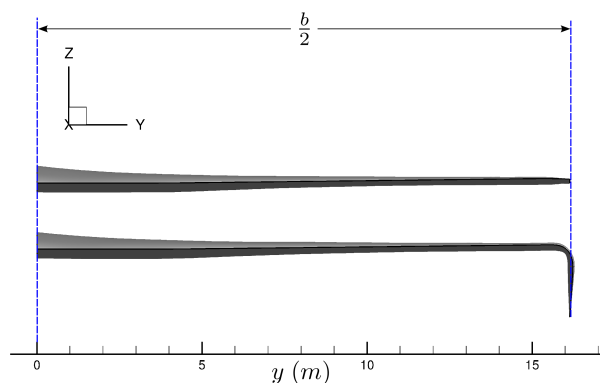


Figure 31: View of the undeflected spans for the planar and winglet-down configurations.

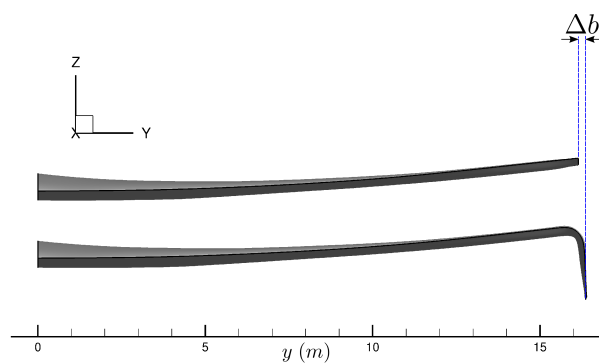


Figure 32: View of the deflected spans for the planar and winglet-down configurations.

most important results of this section. The drag difference relative to the planar wing for each value of β is indicated by ΔD . The inviscid span efficiency factor $e = L^2 / (D_{\text{inviscid}} b^2 q_\infty \pi)$ is also provided, where L is the lift, D_{inviscid} is the inviscid drag, b is the wingspan, and q_∞ is the freestream dynamic pressure. The inviscid drag does not include the friction drag estimate. It is noteworthy that although the span efficiency factor for the wingletted wing with $\beta = 1.0$ is significantly higher than the planar counterpart, it does not translate to a total drag reduction of the same magnitude.

We saw in Section III.B that, from a purely aerodynamic standpoint, the winglet-down configuration is able to push the tip vortex further away from the wing than the winglet-up counterpart. When aerostructural optimization is considered, the winglet-down design pushes the tip vortex even further away from the wing due to the outboard deflection of the winglet-down feature. Figures 31 and 32 demonstrate how the winglet-down configuration has a slightly higher span at the deflected state under the aerodynamic loads. This effect is subtle and is only captured if the structural deflections are taken into account. It is important to note that although the increase in span as a result of the deflections is small, its effect is larger due to the quadratic relation between span and induced drag [28]. This explains why the aerostructural optimizer produces a winglet-down given the freedom to do so. Differences in the projected span values at the deflected state

under the cruise loads relative to the optimized planar cases are indicated by Δb^* in Table 3.

There is an important point about the aerostructural optimization results that we must mention. Although the fully-coupled aerostructural optimization results include more physics than the purely aerodynamic optimization counterparts, we are still largely ignoring the implication of additional critical structural load cases, buckling, and flutter. Consequently, the performance improvements obtained from these results still represent a best-case scenario in the context of practical aircraft design. For instance, adding a winglet may lead to a reduction of the flutter speed by reducing the torsional rigidity of the wing [41, 42]. Similarly, a buckling constraint at the wing-winglet junction of a winglet configuration may overshadow the potential aerodynamic benefit. As a result, if the wingletted wings do not produce a considerable benefit in the absence of such prohibitive constraints, then one can argue that they would not provide greater improvements if we were to take these additional considerations into account. Thus, these results could overestimate the benefits of winglets, but are unlikely to underestimate them.

We have so far limited our discussion of the aerostructural optimization cases to the winglet-down configuration due to the fact that the optimizer seems to favor it over the planar and winglet-up designs. However, there is an important yet subtle point about the winglet-up configuration. The inboard deflection of the winglet-up would bring the tip vortex even closer to the wing relative to the aerodynamically optimal counterpart. This can potentially make the winglet-up configuration less desirable from an aerostructural standpoint. For this reason, it will be interesting to see what the optimizer chooses to do given the freedom to either keep the wing planar or create a winglet-up configuration. Section III.D explores this in more detail.

III.D. Further Investigation Using Aerostructural Optimization

Results from Section III.C indicate that when the aerostructural optimizer is given the freedom to choose the optimal winglet shape at the tip of the wing, it produces a winglet-down configuration. An alternative optimization strategy is to limit the choice of the cant angle in such a way that the optimizer is forced to either produce a nonplanar feature or keep the wing planar for both winglet-up and winglet-down configurations. If the optimizer does not create a winglet in either case, it could be argued that the planar wing is optimal. In this section, we are particularly interested to see if the aerostructural optimizer creates a winglet-up configuration from an initially planar wing for any value of β , especially in light of the fact that this configuration may bring the tip vortex even closer to the wing at the deflected state relative to the purely aerodynamic optimization case.

For the purpose of this investigation we choose the Boeing 737-900 as the baseline aircraft, which is heavier and has a longer fuselage than the one used in the previous sections. This is done in part to gain a

Table 4: Winglet-up and winglet-down optimization design variables

Design Variable	Quantity
Sweep Angle	3
Twist Angle	2
Cant Angle	1
Section Shape	84
Angle of Attack	2
Skin Thickness	60
Spar Thickness	66
Rib Thickness	30
Total	248

better understanding of whether our conclusions are sensitive to the choice of the baseline design. The larger weight leads to a higher lift-induced drag in cruise and could affect the tradeoff between weight and drag. The planform of the initial wing and the corresponding structural wingbox are shown in Figure 15. All of the winglet configurations that are considered have the same undeflected span as the baseline wing and, as a result, have the same planform area as the baseline wing. The projected span of the wing, however, may change due to the structural deflection of the wing. We consider the same cruise and $2.5g$ load conditions as before. The objective function is the same as the one used in Section III.C and is shown in Equation 1. Three values of β have been chosen: 0.5, 0.75, and 1.0. The optimizations are conducted in a single stage using the grid with 653,184 nodes in 112 blocks. Based on our investigations in the previous sections, there is practical justification for ending the optimization cases after approximately 150 design iteration as the majority of the reduction in the merit function will be achieved.

The nonlinear constraints used in this investigation are the same as the ones listed in Table 1. However, the total weight of the aircraft is assumed to be equal to the computed weight of the wing plus a fixed weight of 785,000 N. This fixed weight is estimated based on the maximum takeoff weight of a Boeing 737-900 excluding the approximate wing weight. The structural sizing methodology is the same as before. Table 4 provides a list of the design variables used for winglet-up and winglet-down optimization cases. These cases have a total of 248 design variables. The geometric parameterization is slightly different from the previous sections in that the sectional shape is controlled at fewer spanwise stations to reduce the number of design variables. Figure 33 shows the geometric design variables that control the shape of the wing and winglet. The optimizer has the freedom to change the sectional shape of the wing by manipulating the z -coordinates of the control points at 6 spanwise stations. The airfoil shapes are interpolated between these stations using the remaining control points. For a winglet-up configuration to form from an initially planar wing, the cant angle at the wingtip is allowed to vary between 0 and $+90^\circ$. Similarly, for a winglet-down configuration, the optimizer is free to vary the cant angle between 0 and -90° . In both cases, the optimizer is free to keep the

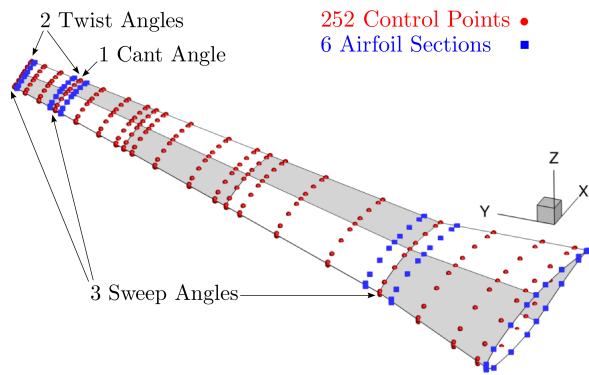


Figure 33: Geometric parameterization and design variables.

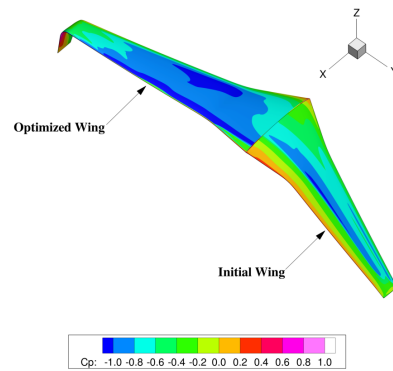


Figure 34: The optimized winglet-down configuration with $\beta = 0.5$ along with the initial wing.

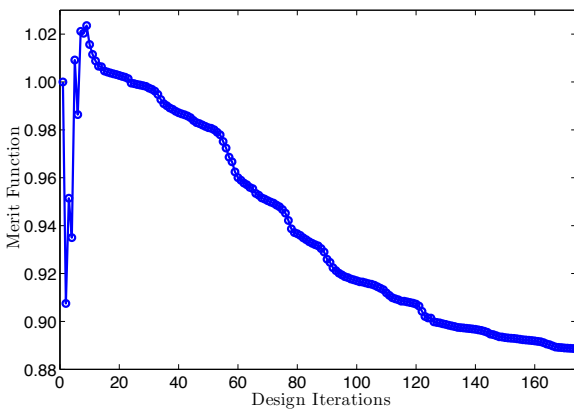


Figure 35: Merit function convergence history for the winglet-down configuration with $\beta = 1.0$.

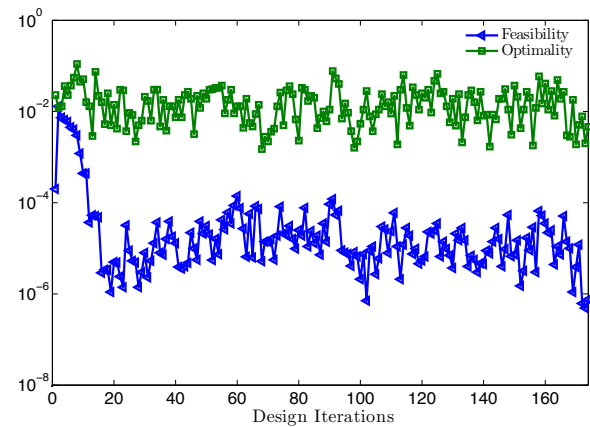


Figure 36: Feasibility and optimality convergence histories for the winglet-down configuration with $\beta = 1.0$.

wing planar. The maximum height of the nonplanar feature at the wingtip is constrained to 6% of the wing span. For the planar wing optimization case, the wingtip cant angle design variable is inactive and hence the optimizer does not have the freedom to create a nonplanar feature at the tip of the wing. As an example, Figure 34 shows the optimized winglet-down configuration with $\beta = 0.5$ along with the initial wing.

Figure 35 shows the merit function history for the winglet-down configuration with $\beta = 1.0$. Figure 36 shows the corresponding convergence histories for optimality and feasibility. These aerostructural optimization cases tend to converge rather slowly [43]. Nevertheless, Figure 35 indicates that we have obtained the majority of the merit function improvement. The optimizer completed 174 design iterations in 6 days of walltime on 240 processors. These general convergence trends hold true for the rest of the optimization cases as well.

Figure 37 shows plots of the pressure coefficient on the top surface for the initial geometry evaluated on the fine mesh. Plots of the pressure coefficient for the optimized winglet-down configuration with $\beta = 0.75$ are shown in Figure 38. The initial geometry does not satisfy the nonlinear lift constraint using the initial

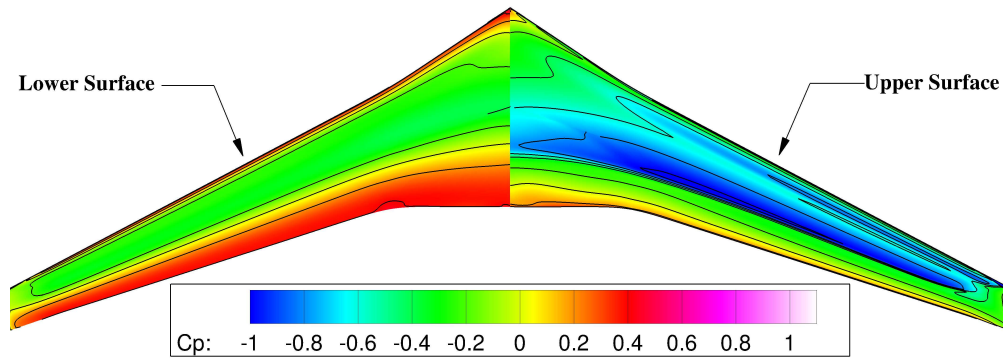


Figure 37: Contours of pressure coefficient on the upper and lower surfaces for the initial geometry.

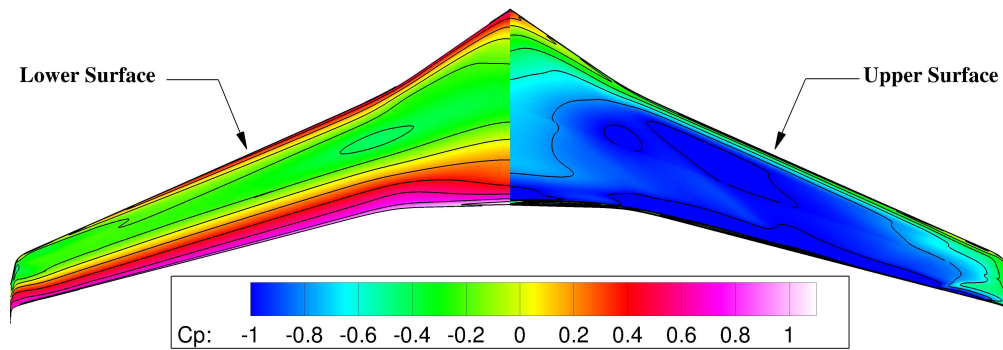


Figure 38: Pressure coefficient contours for the optimized winglet-down configuration with $\beta = 0.75$.

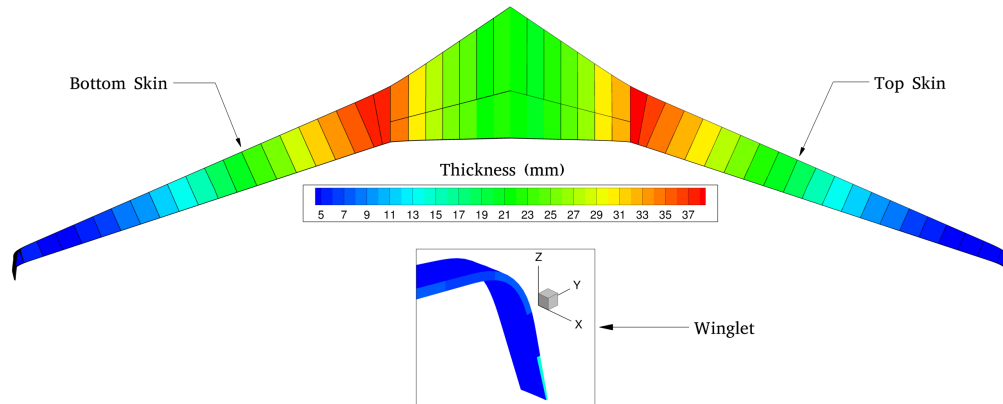


Figure 39: Skin thickness values in millimeters for the winglet-down configuration with $\beta = 0.75$.

value of the angle of attack and leads to a shock that is present over a large portion of the upper surface. The optimizer has eliminated this shock on the upper surface of the optimized design while satisfying all nonlinear constraints to a tolerance of 10^{-6} .

The optimized skin thickness values for the winglet-down configuration are shown in Figure 39. Note that the aerostructural optimization has thickened the skin inboard. This is somewhat expected because the failure criterion at the $2.5g$ load condition tends to be closer to the critical value at the root of the wing and near the crank, as shown in Figure 40. The optimized thickness distributions for the ribs and spars follow

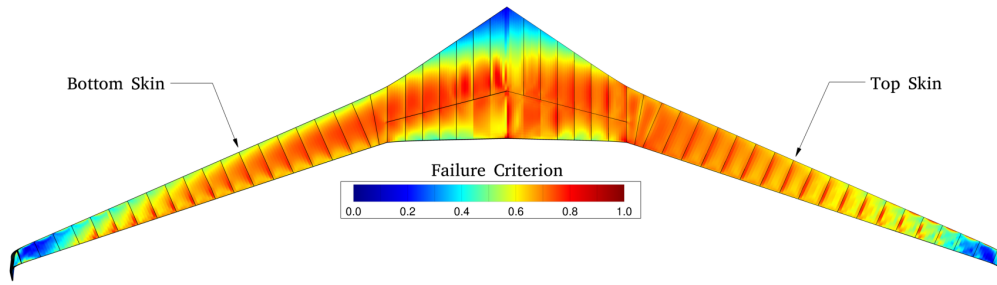


Figure 40: Plot of the von Mises failure criterion at the 2.5g load condition for the winglet-down configuration with $\beta = 0.75$. A value of unity indicates structural failure.

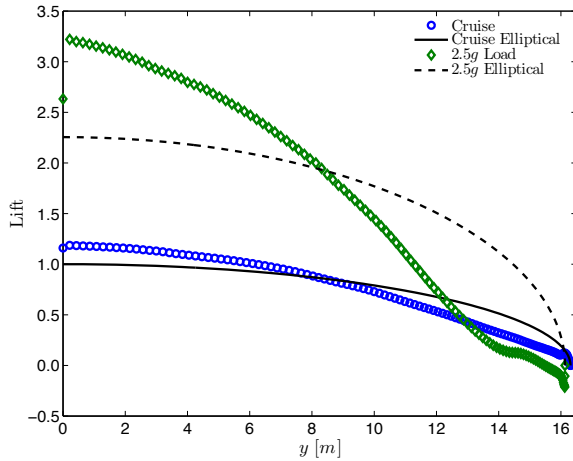


Figure 41: Spanwise lift distributions at cruise and 2.5g load conditions for the winglet-down configuration with $\beta = 0.5$.

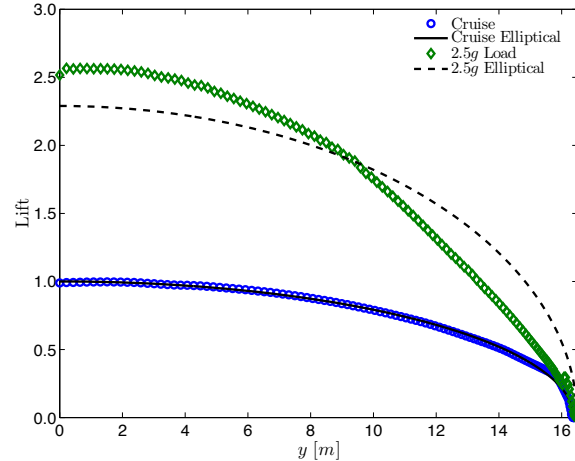


Figure 42: Spanwise lift distributions at cruise and 2.5g load conditions for the winglet-down configuration with $\beta = 1.0$.

a similar pattern. Although we have not considered all of the necessary critical load conditions that are required in the context of wing design, this result shows that we have captured at least some of the correct trends dictated by the structural sizing of the wing.

The weight of the baseline aircraft considered in this section is significantly larger than the one in Section III.C. In order to show that the optimizer can recover the fundamental tradeoff between weight and drag correctly regardless of the baseline maximum takeoff weight, we examine the optimized lift distributions as well as the planform shapes. Figure 41 shows the spanwise lift distributions for the cruise and 2.5g load conditions corresponding to the winglet-down configuration with $\beta = 0.5$. These have been normalized with respect to the lift at the root for an elliptical lift distribution at cruise. The optimizer is aeroelastically tailoring the wing in order to significantly reduce the tip loading at the 2.5g load condition while maintaining a lift distribution closer to elliptical for the wing at the cruise condition. Figure 42 shows the spanwise lift distributions for the winglet-down configuration with $\beta = 1.0$. In this case, the cruise lift distribution more closely follows the elliptical lift distribution than the $\beta = 0.5$ case. Furthermore, the tip loading at the 2.5g load condition is greater in comparison to the $\beta = 0.5$ result. In other words, the optimizer is further

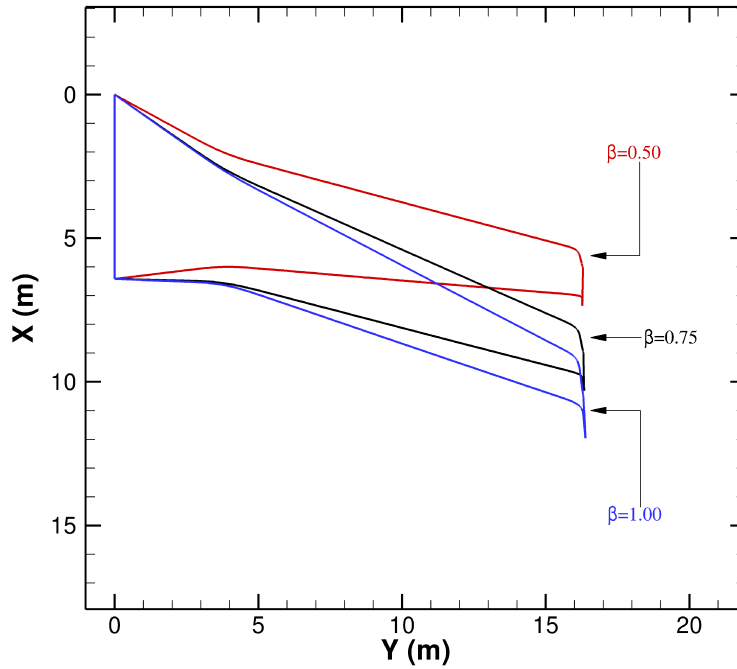


Figure 43: Top-down view of the optimal winglet-down configurations.

reducing the cruise drag at the cost of increasing the wing weight. Thus, the optimizer has captured the expected tradeoff between weight and drag.

Figure 43 shows the top-down view of optimal designs for the winglet-down configuration. The values of β are also provided. As the value of β increases from 0.5 to 1.0, i.e. as we place increasing emphasis on the drag in the objective function, the sweep angles of the wings also increase. This is the expected trend because wing sweep reduces wave drag. The same trend exists for the planar configurations.

Figure 44 shows the tradeoff curves of the optimal solutions obtained for all of the configurations considered. The optimized planar wing with $\beta = 0.5$ has a normalized drag value equal to unity. Similarly, the optimized planar wing with $\beta = 1.0$ has a normalized weight value equal to unity. Note that for the purpose of this plot, the weight values are obtained by adding the calculated wing weight to a fixed weight of 785,000 N to get an approximate total aircraft weight. Similarly, the drag values are obtained by adding the calculated inviscid drag based on the Euler equations to a friction drag estimate of the entire aircraft based on the same methodology used in Section III.B. In this case, we estimate that the friction drag at cruise is equal to 200 drag counts for the baseline planar configuration due to the longer fuselage length [32, 33]. In all cases, as we place increasing emphasis on inviscid drag in the objective function, i.e. as we vary β from 0.5 to 1.0, the drag decreases at the cost of increasing weight.

Figure 44 shows that the winglet-down configuration can provide a total drag reduction of up to 2% for the same weight in comparison to the planar wings. Although the reduction in inviscid drag is as high as 8% at the same weight, the increase in the surface area due to the nonplanar feature at the tip reduces the

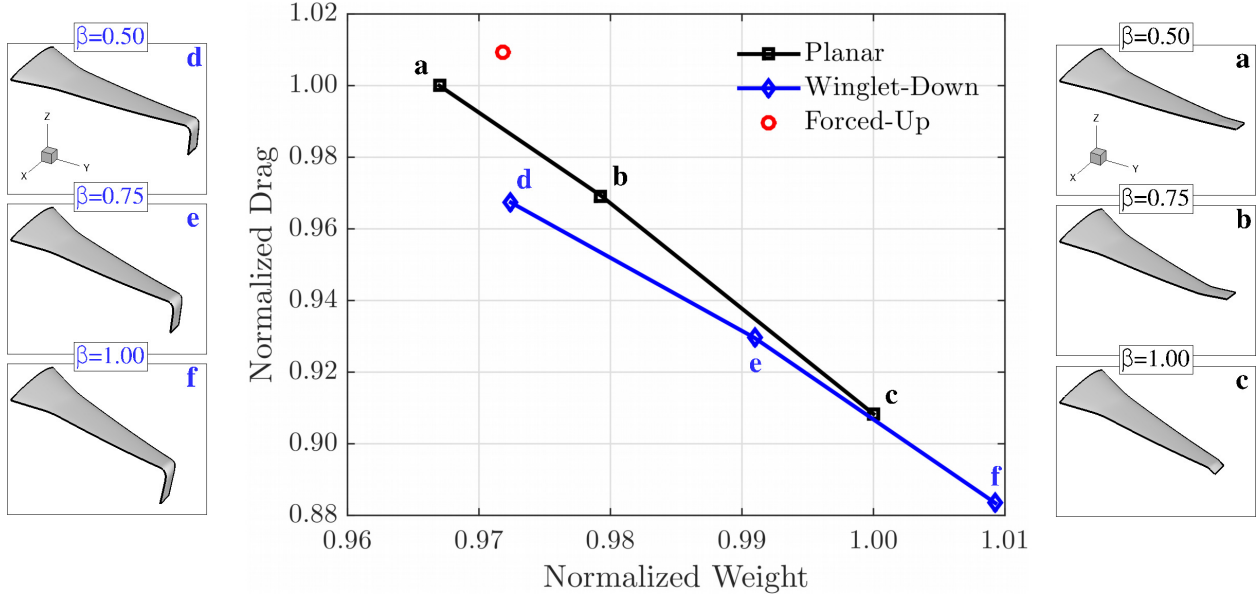


Figure 44: Tradeoff curves of optimal designs for all of the wingletted and planar configurations considered.

Table 5: Summary of the aerostructural optimization results obtained from the fine grid

<i>Parameter</i>	Planar			Winglet-Down		
	$\beta = 0.50$	$\beta = 0.75$	$\beta = 1.00$	$\beta = 0.50$	$\beta = 0.75$	$\beta = 1.00$
C_L	0.576	0.587	0.596	0.581	0.594	0.603
Total drag (counts)	412	400	374	399	383	364
ΔD	0.0%	0.0%	0.0%	-3.2%	-4.3%	-2.7%
L/D	14.0	14.7	15.6	14.6	15.1	16.6
Δb^*	0.0%	0.0%	0.0%	1.1%	1.3%	1.5%
$W (\times 10^5 \text{ N})$	2.91	3.44	4.33	3.15	3.94	4.73
e	0.782	0.863	0.981	0.870	0.991	1.143

total drag improvement and the winglet adds weight as well, which increases the induced drag due to the higher lift coefficient needed. Figure 44 does not include the winglet-up results^a because the optimizer did not create a winglet-up feature for any of the β values even though it did have the geometric freedom to do so. In other words, when the optimizer has the freedom to create a winglet-up feature, it chooses to keep the wing planar regardless of the value of β . On the other hand, the optimizer produces a winglet-down feature for each value of β when it is given the freedom to do so. This reaffirms our original findings presented in Section III.C. Table 5 summarizes the results obtained from the fine mesh analysis.

Although the aerostructural optimizer does not create a winglet-up configuration given the freedom to do so, it is important to eliminate the possibility that the winglet-up performs better than the planar wing or the winglet-down configuration. In order to address this, we have run an optimization case where the

^aThe forced winglet-up case will be discussed in the following paragraph.

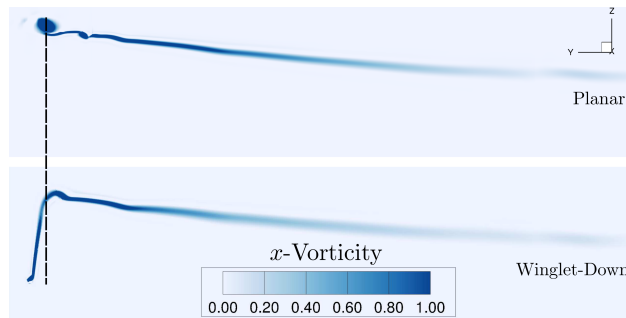


Figure 45: Contours of x -vorticity behind the trailing edge of the wing for the planar and winglet-down cases. The dashed line marks the location of the tip vortex for the planar configuration.

cant angle is forced to be equal to $+90^\circ$. This case is depicted by the red circle in Figure 44. It is clear that this design is dominated by the planar and winglet-down configurations. This provides additional evidence that the winglet-up configuration is not better than the planar wing or the winglet-down configuration. The reader is reminded that even from a purely aerodynamic perspective, the winglet-up configuration reduces the total drag only by 1.1% in comparison to an optimal planar wing of the same span, as shown in Section III.B. From an aerostructural perspective, this configuration reduces the projected span at the deflected state and brings the tip vortex closer to the wing. Furthermore, the addition of the winglet adds weight both by increasing the structural span and modifying the tip loading. The combination of these effects make the winglet-up configuration have inferior performance relative to its planar counterpart.

The winglet-down configuration performs better than the planar and winglet-up counterparts for two reasons. First, this design moves the tip vortex further away from the wing even when the deflections are not taken into account. Second, the projected span of the winglet-down configuration at the deflected state is in fact larger than its planar and winglet-up counterparts. The tip vortex moves even further away from the wing in comparison to the purely aerodynamic optimization case. This highlights the importance of capturing the deflected shape of the wing under the aerodynamic loads. We have reached the same conclusion even when using different geometry parameterization and mesh movement schemes for the purpose of optimization [44]. In the case of a winglet-up configuration, the structural deflection reduces the projected span and brings the tip vortex closer to the wing. From an aerostructural perspective, this leads to a higher objective function for the winglet-up configuration relative to the planar counterpart.

Figure 45 shows that the winglet-down configuration pushes the tip vortex further away from the wing in the positive y -direction in comparison to the optimized planar wing of the same projected span. This means that the induced downwash is reduced in the winglet-down case. As a result, the induced drag is lower.

Although the winglet-down configuration appears to be the most competitive design, its relative drag benefit in comparison to the planar wing is smaller than those reported in past studies based on purely aerodynamic shape optimization that considered low-speed flying conditions [30]. Furthermore, our results

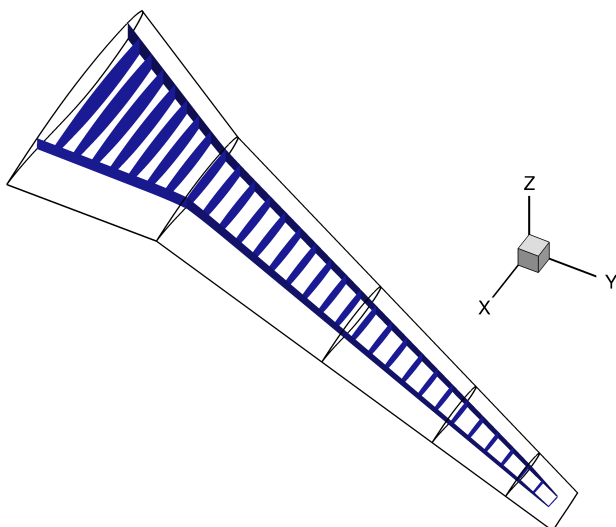


Figure 46: Primary structural layout of the ribs and spars used for the purpose of this investigation.

indicate that at least some of the induced drag advantage of the winglet-down configuration is due to the increased span of the wing at the deflected state. This suggests that perhaps we should include other phases of a commercial flight profile such as the steady climb, where the ratio of induced to total drag is higher than in cruise. We will explore this in Section III.E.

III.E. Optimal Winglets for Cruise and Climb Conditions

The main objective of this section is to explore the possibility that wingletted wings may provide a larger benefit in high-lift, low-speed conditions. The induced drag constitutes up to 80% of the total drag of the aircraft in high-lift, low-speed conditions such as takeoff [1]. This is largely due to the fact that the coefficient of lift is larger than in cruise. The aerostructural analysis and optimization framework used in this work does not have the capability to analyze a takeoff condition, but we are indeed able to study other low-speed, high-lift conditions including steady climb.

The optimization problem formulation in terms of the initial geometry and geometric design variables and parameterization is the same as the one in Section III.C, but the structural layout is slightly simpler, as shown in Figure 46. There is now an additional representative steady climb condition where the Mach number is equal to 0.40 at an altitude of 10,000 ft. The objective function is the sum of the total drag in cruise and climb conditions. This choice of objective function may not be practical, but is effective in studying the most important trends that we are interested in.

Table 6 shows the comparison of the total drag reduction from the optimal wingletted wing in comparison to the planar configuration with the climb condition included in the optimization as a design point. The nonplanar optimization produces a winglet-down configuration when the optimizer is given the freedom to

Table 6: Comparison of total drag reduction in cruise and climb conditions for the optimal winglet-down configuration

Flying Condition	Total Drag Reduction
Cruise	2.5%
Climb	3.7%

Table 7: The ratio of induced to total drag for the optimal winglet-down configuration in the cruise and climb conditions

Flying Condition	$D_{induced}/D_{total}$
Cruise	0.35
Climb	0.45

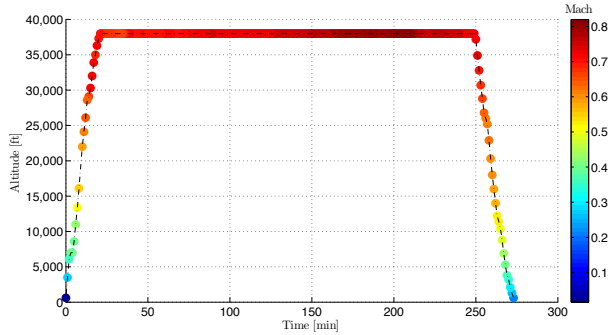


Figure 47: The flight profile of a B737NG aircraft from Toronto to Vancouver.

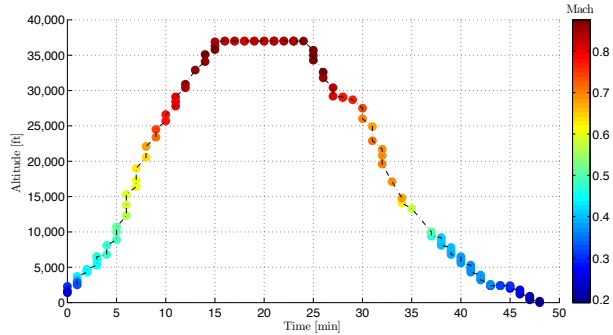


Figure 48: The flight profile of a B737NG aircraft from Toronto to Montreal.

do so. It is clear that the nonplanar wing is providing a higher drag reduction in climb than in cruise. This is due to the fact that the ratio of the induced to total drag is higher in climb than in cruise, as shown in Table 7. Therefore, the friction drag penalty associated with the increased surface area of the wingletted design is lower in comparison to cruise. In other words, any induced drag reduction provided by the winglet has a greater influence on the total drag value.

The most important conclusion from our climb optimization study is that a wingletted wing may provide a larger total drag reduction in high-lift, low-speed conditions such as steady climb. Thus, whether or not a particular winglet configuration can help reduce the total drag of an aircraft significantly may depend on its intended mission profile in addition to the choice of the objective function it is optimized for. To further illustrate this point, Figure 47 shows the flight profile of a B737NG aircraft from Toronto to Vancouver, where the distance flown is approximately 3,600 km^b. It is clear that the time spent during the climb and descent segments are significantly shorter in comparison to cruise. This suggests that perhaps a wingletted wing may not provide a significant drag reduction for this flight profile. However, the same aircraft is also used on shorter routes such as the one shown in Figure 48, where the distance flown is just under 600 km. In this case, the aircraft spends a significant amount of time in low-speed, high-lift conditions relative to cruise and as a result, a wingletted wing may be more useful.

^bFlight information obtained from publicly available data at <https://flightaware.com/>

IV. Conclusions

This paper provides an aerostructural perspective on the potential efficiency gains from wingletted wings. Three configurations are considered: winglet-up, winglet-down, and planar. A step-by-step approach is adopted where these configurations are first assessed using purely aerodynamic shape optimization based on the Euler equations along with a friction drag estimate based on the wetted surface area. Fully-coupled aerostructural optimization is subsequently performed to take into account the effects of structural weight and deflection in addition to drag. The most important conclusions are listed below.

1) From a purely aerodynamic perspective, winglets oriented downward produce a larger drag reduction than winglets oriented upward by moving the tip vortex further away from the wing in the spanwise direction.

2) When fully-coupled aerostructural optimization is considered, the results indicate that the winglet-down configuration is able to push the tip vortex even further away from the wing relative to the purely aerodynamic case by increasing the projected span at the deflected state. This configuration reduces the drag at the same total weight by 2% in comparison to the planar counterpart.

3) Purely aerodynamic shape optimization results show that the winglet-up configuration reduces the total drag by 1.1% in comparison to an optimized planar wing of the same projected span. From an aerostructural perspective, however, this configuration brings the tip vortex closer to the wing due to the inboard deflection of the winglet feature. Furthermore, the addition of the winglet adds weight to the wing by changing the spanwise loading and increasing the structural span. The combination of these effects make the winglet-up design inferior to an optimized planar wing of the same span.

4) Our results indicate that the potential benefits of wingletted wings are larger in low-speed, high-lift conditions such as the steady climb because the ratio of induced to total drag is higher than in cruise.

Acknowledgments

The authors acknowledge Prof. Joaquim R. R. A. Martins of the University of Michigan, Ann Arbor for sharing his framework for the purpose of constructing our methodology. Furthermore, the authors gratefully acknowledge the financial support provided by the Ontario Graduate Scholarship program, the National Science and Engineering Research Council, and the University of Toronto. Computations were performed on the GPC supercomputer at the SciNet HPC Consortium. SciNet is funded by the Canada Foundation for Innovation under the auspices of Compute Canada, the Government of Ontario, Ontario Research Fund - Research Excellence, and the University of Toronto.

References

- ¹ Kroo, I., “Drag Due to Lift: Concepts for Prediction and Reduction,” *Annual Review of Fluid Mechanics*, Vol. 33, No. 1, 2001, pp. 587–617.
- ² Whitcomb, R., “A Design Approach and Selected Wind Tunnel Results at High Subsonic Speeds for Wing-Tip Mounted Winglets,” Tech. Rep. TN-D-8260, NASA, 1976.
- ³ Heyson, H. H., Riebe, G. D., and Fulton, C. L., “Theoretical Parametric Study of the Relative Advantages of Winglets and Wing-Tip Extensions,” Tech. Rep. TP-1020, NASA, 1977.
- ⁴ Jones, R. T. and Lasinsky, T. A., “Effects of Winglets on the Induced Drag of Ideal Wing Shapes,” Tech. Rep. TM-81230, NASA, 1980.
- ⁵ Asai, K., “Theoretical Considerations in Aerodynamic Effectiveness of Winglets,” *Journal of Aircraft*, Vol. 22, No. 7, 1985, pp. 635–637.
- ⁶ van Dam, C. P., “Induced-Drag Characteristics of Crescent-Moon-Shaped Wings,” *Journal of Aircraft*, Vol. 24, No. 2, 1987, pp. 115–119.
- ⁷ Smith, S. C. and Kroo, I., “Computation of Induced Drag for Elliptical and Crescent-Shaped Wings,” *Journal of Aircraft*, Vol. 30, No. 4, 1993, pp. 446–452.
- ⁸ Takenaka, K. and Hatanaka, K., “Multidisciplinary Design Exploration for a Winglet,” *Journal of Aircraft*, Vol. 45, No. 5, 2008, pp. 1601–1611.
- ⁹ Verstraeten, J. G. and Slingerland, R., “Drag Characteristics for Optimally Span-Loaded Planar, Wingletted, and C Wings,” *Journal of Aircraft*, Vol. 46, No. 3, 2009, pp. 962–971.
- ¹⁰ Ning, S. A. and Kroo, I., “Multidisciplinary Considerations in the Design of Wings and Wing Tip Devices,” *Journal of Aircraft*, Vol. 47, No. 2, 2010, pp. 534–543.
- ¹¹ Jansen, P., Perez, R. E., and Martins, J. R. R. A., “Aerostructural Optimization of Nonplanar Lifting Surfaces,” *Journal of Aircraft*, Vol. 47, No. 5, 2010, pp. 1491–1503.
- ¹² Faye, R., Laprete, R., and Winter, M., “Blended Winglets for Improved Airplane Performance,” Tech. rep., Boeing Commercial Airplanes, http://www.boeing.com/commercial/aeromagazine/aero_17/winglets.pdf.
- ¹³ Koo, D. and Zingg, D. W., “Progress in Aerodynamic Shape Optimization Based on the Reynolds-Averaged Navier-Stokes Equations,” *The AIAA Science and Technology Forum and Exposition (AIAA SciTech)*, San Diego, California, January 2016.

- ¹⁴ Kennedy, G. J. and Martins, J. R. R. A., “A Comparison of Metallic and Composite Aircraft Wings Using Aerostructural Design Optimization,” *14th AIAA/ISSMO Multidisciplinary Analysis and Optimization Conference*, Indianapolis, IN, sep 2012, AIAA-2012-5475.
- ¹⁵ Kenway, G. K. W., Kennedy, G. J., and Martins, J. R. R. A., “Aerostructural optimization of the Common Research Model configuration,” *15th AIAA/ISSMO Multidisciplinary Analysis and Optimization Conference*, Atlanta, Georgia, June 2014.
- ¹⁶ Hicken, J. E. and Zingg, D. W., “Parallel Newton-Krylov Solver for the Euler Equations Discretized Using Simultaneous-Approximation Terms,” *AIAA Journal*, Vol. 46, No. 11, 2008, pp. 2773–2786.
- ¹⁷ Osusky, M. and Zingg, D. W., “Parallel Newton-Krylov-Schur Solver for the Navier-Stokes Equations Discretized Using Summation-By-Parts Operators,” *AIAA Journal*, Vol. 51, No. 12, 2013, pp. 2833–2851.
- ¹⁸ Kennedy, G. J. and Martins, J. R. R. A., “A parallel finite-element framework for large-scale gradient-based design optimization of high-performance structures,” *Finite Elements in Analysis and Design*, Vol. 87, September 2014, pp. 56–73.
- ¹⁹ Hicken, J. E. and Zingg, D. W., “Aerodynamic Optimization Algorithm with Integrated Geometry Parameterization and Mesh Movement,” *AIAA Journal*, Vol. 48, No. 2, 2010, pp. 400–413.
- ²⁰ Zhang, Z. J., Khosravi, S., and Zingg, D. W., “High-Fidelity Aerostructural Optimization with Integrated Geometry Parameterization and Mesh Movement,” *56th AIAA/ASCE/AHS/ASC Structures, Structural Dynamics, and Materials Conference*, No. AIAA 2015-1132, Kissimmee, Florida, January 2015.
- ²¹ Zhang, Z. J., Khosravi, S., and Zingg, D. W., “High-Fidelity Aerostructural Optimization with Integrated Geometry Parameterization and Mesh Movement,” *Structural and Multidisciplinary Optimization*, 2016, Accepted.
- ²² Gill, P. E., Murray, W., Michael, and Saunders, M. A., “SNOPT: An SQP Algorithm For Large-Scale Constrained Optimization,” *SIAM Journal on Optimization*, Vol. 12, 1997, pp. 979–1006.
- ²³ Perez, R. E., Jansen, P. W., and Martins, J. R. R. A., “pyOpt: A Python-Based Object-Oriented Framework for Nonlinear Constrained Optimization,” *Structural and Multidisciplinary Optimization*, Vol. 45, No. 1, 2012, pp. 101–118.
- ²⁴ Kennedy, G. J. and Martins, J. R. R. A., “Parallel Solution Methods for Aerostructural Analysis and Design Optimization,” *13th AIAA/ISSMO Multidisciplinary Analysis Optimization Conference*, No. AIAA-2010-9308, Fort Worth, Texas, September 2010.

- ²⁵ Zingg, D. W., Nemec, M., and Pulliam, T. H., “A comparative evaluation of genetic and gradient-based algorithms applied to aerodynamic optimization,” *Revue européenne de mécanique numérique*, Vol. 17, No. 1-2, March 2008, pp. 103–126.
- ²⁶ Chernukhin, O. and Zingg, D. W., “Multimodality and Global Optimization in Aerodynamic Design,” *AIAA Journal*, Vol. 51, No. 6, 2013, pp. 1342–1354.
- ²⁷ Martins, J. R. R. A., Alonso, J. J., and Reuther, J. J., “A Coupled-Adjoint Sensitivity Analysis Method for High-Fidelity Aero-Structural Design,” *Optimization and Engineering*, Vol. 6, 2005, pp. 33–62.
- ²⁸ Anderson, J. D., *Fundamentals of Aerodynamics*, McGraw-Hill, 1221 Avenue of the Americas, New York, NY 10020, United States of America, 4th ed., 2007.
- ²⁹ “737 Airplane Characteristics for Airport Planning,” Tech. rep., Boeing Commercial Airplanes, September 2013, <http://www.boeing.com/assets/pdf/commercial/airports/acaps/737.pdf>.
- ³⁰ Hicken, J. E. and Zingg, D. W., “Induced-Drag Minimization of Nonplanar Geometries Based on the Euler Equations,” *AIAA Journal*, Vol. 48, No. 11, 2010, pp. 2564–2575.
- ³¹ Gagnon, H. and Zingg, D. W., “Two-Level Free-Form and Axial Deformation for Exploratory Aerodynamic Shape Optimization,” *AIAA Journal*, Vol. 53, No. 7, 2015, pp. 2015–2026.
- ³² Fredericks, W., Costa, K. A. G., Deshpande, N., Moore, M., Miguel, E. S., and Snyder, A., “Aircraft Conceptual Design Using Vehicle Sketch Pad,” *48th AIAA Aerospace Sciences Meeting Including the New Horizons Forum and Aerospace Exposition*, No. AIAA 2010-658, Orlando, Florida, January 2010.
- ³³ Gur, O., Mason, W. H., and Schetz, J. A., “Full-Configuration Drag Estimation,” *Journal of Aircraft*, Vol. 47, No. 4, 2010, pp. 1356–1367.
- ³⁴ Bourdin, P., “NUMERICAL PREDICTIONS OF WING-TIP EFFECTS ON LIFT-INDUCED DRAG,” *International Council of Aeronautical Sciences (ICAS) Congress*, No. 2002-2.2.3, Toronto, Ontario, September 2002.
- ³⁵ Kenway, G. K. W., Kennedy, G. J., and Martins, J. R. R. A., “A CAD-Free Approach to High-Fidelity Aerostructural Optimization,” *Proceedings of the 13th AIAA/ISSMO Multidisciplinary Analysis Optimization Conference*, Fort Worth, Texas, September 2010, AIAA 2010-9231.
- ³⁶ Wrenn, G. A., “An Indirect Method for Numerical Optimization Using the Kreisselmeier–Steinhauser Function,” Tech. Rep. CR-4220, NASA, 1989.

- ³⁷ Akgün, M. A., Haftka, R. T., Wu, K. C., Walsh, J. L., and Garcelon, J. H., “Efficient Structural Optimization for Multiple Load Cases Using Adjoint Sensitivities,” *AIAA Journal*, Vol. 39, No. 3, 2001, pp. 511–516.
- ³⁸ Martins, J. R. R. A., Alonso, J. J., and Reuther, J. J., “High-Fidelity Aerostructural Design Optimization of a Supersonic Business Jet,” *Journal of Aircraft*, Vol. 41, No. 3, 2004, pp. 523–530.
- ³⁹ Kennedy, G. J., *Aerostructural Analysis and Design Optimization of Composite Aircraft*, Ph.D. thesis, University of Toronto, September 2012.
- ⁴⁰ Osusky, L., Buckley, H., Reist, T., and Zingg, D. W., “Drag Minimization Based on the Navier-Stokes Equations Using a Newton-Krylov Approach,” *AIAA Journal*, Vol. 53, No. 6, June 2015, pp. 1555–1577.
- ⁴¹ Cui, P. and Han, J., “Prediction of flutter characteristics for a transport wing with wingtip devices,” *Aerospace Science and Technology*, Vol. 23, No. 1, 2012, pp. 461–468.
- ⁴² Snyder, M. P. and Weisshaar, T. A., “Flutter and Directional Stability of Aircraft with Wing-Tip Fins: Conflicts and Compromises,” *Journal of Aircraft*, Vol. 50, No. 2, 2013, pp. 615–625.
- ⁴³ Kenway, G. K. W., Kennedy, G. J., and Martins, J. R. R. A., “Multipoint High-Fidelity Aerostructural Optimization of a Transport Aircraft Configuration,” *Journal of Aircraft*, Vol. 51, 2014, pp. 144–160.
- ⁴⁴ Khosravi, S. and Zingg, D. W., “A Numerical Optimization Study on Winglets,” *15th AIAA/ISSMO Multidisciplinary Analysis and Optimization Conference*, No. AIAA 2014-2173, Atlanta, Georgia, June 2014.